Disruption of MDA5 mediated innate immune responses by the 3C proteins of Coxsackievirus A16, Coxsackievirus A6, and Enterovirus D68

Yajuan Rui,[a,b,c] Jiaming Su,[a,b,c,d] Hong Wang,[a] Junliang Chang,[a] Shaohua Wang,[a] Wenwen Zheng,[a] Yong Cai,[c] Wei Wei,[a] James T. Gordy[b], Richard Markham,[b] Wei Kong,[c] Wenyan Zhang,[a*] and Xiao-Fang Yu[a,b,d*]

First Hospital of Jilin University, Institute of Virology and AIDS Research, Changchun, Jilin Province, China[a]; Department of Molecular Microbiology and Immunology, Johns Hopkins Bloomberg School of Public Health, 615 N. Wolfe Street, Baltimore, MD 21205, USA[b]; School of Life Sciences, Jilin University, Changchun, Jilin Province, China[c] ; Cancer Institute (Key Laboratory of Cancer Prevention and Intervention, China National Ministry of Education), The Second Affiliated Hospital, Zhejiang University School of Medicine, Hangzhou, Zhejiang 310009, China[d]

Corresponding author: Prof. Xiao-Fang Yu, Department of Molecular Microbiology and Immunology, Johns Hopkins Bloomberg School of Public Health, 615 N. Wolfe Street, Baltimore, MD 21205, USA. E-mail address: xyu2@jhu.edu

Prof. Wenyan Zhang: zhangwenyan@jlu.edu.cn

Running title: $3C^{pro}$ inhibits MDA5 mediated cellular defense

ABSTRACT

Coxsackievirus A16 (CV-A16), A6 (CV-A6), and enterovirus D68 (EV-D68) belong to the *Picornaviridae* family and are major causes of hand, foot, and mouth disease (HFMD) and pediatric respiratory disease worldwide. The biological characteristics of these viruses, especially their interplay with the host innate immune system, have not been well investigated. In this study, we discovered that the $3C^{pro}$ proteins from CV-A16, CV-A6, and EV-D68 bind MDA5 and inhibit its interaction with MAVS. Consequently, MDA5-triggered type I IFN signaling in the RLR pathway was blocked by CV-A16, CV-A6, and EV-D68 $3C^{pro}$. Furthermore, CV-A16, CV-A6, and EV-D68 $3C^{pro}$ all cleave TAK1, resulting in inhibition of NF-κB activation, a host response also critical for toll-like receptor (TLR) mediated signaling. Thus, our data demonstrate that circulating HFMD-associated CV-A16 and CV-A6, as well as severe respiratory disease-associated EV-D68, have developed novel mechanisms to subvert host innate immune responses by targeting key factors in the RLR and TLR pathways. Blocking the ability of $3C^{pro}$ from diverse enteroviruses and coxsackieviruses to interfere with type I IFN induction should restore IFN anti-viral function, offering a potential novel anti-viral strategy.

Key words: MDA5; TAK1; MAVS; 3C protease; CV-A16; CV-A6; EV-D68; HFMD; innate immune response

IMPORTANCE

CV-A16, CV-A6, and EV-D68 are emerging pathogens associated with hand, foot, and mouth disease and pediatric respiratory disease worldwide. The pathogenic mechanisms of these viruses are largely unknown. Here we demonstrate that the CV-A16, CV-A6, and EV-D68 $3C^{pro}$ protease blocks MDA5-triggered type I IFN induction. $3C^{pro}$ of these viruses binds MDA5 and inhibits its interaction with MAVS. In addition, CV-A16, CV-A6, and EV-D68 $3C^{pro}$ cleaves TAK1 to inhibit the NF-κB response. Thus, our data demonstrate that circulating HFMD-associated CV-A16 and CV-A6, as well as severe respiratory disease-associated EV-D68, have developed a mechanism to subvert host innate immune responses by simultaneously targeting key factors in the RLR and TLR pathways. These findings indicate the potential merit of targeting CV-A16, CV-A6, and EV-D68 $3C^{pro}$ as an anti-viral strategy.

INTRODUCTION

Hand, foot, and mouth disease (HFMD) is a common infectious disease among young children. Enterovirus 71 (EV-A71, EV71) and coxsackievirus A16 (CV-A16, CA16) are most frequently associated with HFMD worldwide. Extensive studies have focused on EV-A71 because of its association with severe complications involving the central nervous system and significant mortality (1, 2). However, since the CV-A16-related outbreak of HFMD occurred in England in 1994 (3), accumulating evidence has demonstrated that CV-A16 infection can also cause severe neurological complications (4) and death (5, 6). Recently, coxsackievirus A6 (CV-A6) infection has also been increasingly associated with HFMD outbreaks around the world (7-17). Further, enterovirus D68 (EV-D68) has been linked to severe respiratory disease worldwide in recent years. To date, no effective vaccines or treatments for enterovirus or coxsackie virus infection are available.

The interferon induction pathway is commonly targeted by viruses. Host cells orchestrate the production of type I interferons (IFNs) upon detection of invading viral pathogens. To antagonize viral invasion, pathogen-associated molecular patterns (PAMPs) are sensed by cellular pattern recognition receptors (PRRs) to activate the type I IFN induction signaling pathway (18, 19). The retinoic acid-inducible gene-I-like receptors (RLRs), are PRRs that play a pivotal role in the innate immune system. The members of the RLR family, including Retinoic Acid Inducible Gene-I (RIG-I), Melanoma Differentiation-Associated gene 5 (MDA5), and Laboratory of Genetics and Physiology 2 (LGP2), are located in the cytoplasm and monitor for the presence of viral RNA (20). RIG-I and MDA5 belong to the family of DExD/H box RNA helicases that contain two caspase-activation and recruiting domains (CARD) at their N termini

and a single DExD/H box RNA helicase domain at their C termini (CTD). Upon RNA viral infection, the CTD domains of RIG-I and MDA5 sense viral RNA that bears a 5'-triphosphate group and long kilobase-scale genomic RNA, respectively, which are both lacking in host mRNA (21-26). After binding viral RNA, RIG-I and MDA5 undergo conformational changes and transduce signals to the downstream adaptor MAVS (virus-induced signaling adapter, also named VISA, Cardif or IPS-1) (27-29) through a CARD-CARD interaction. As a result, TRAFs, IKKε, and TBK1 are recruited by the MAVS signaling complex. IKKε and TBK1 then phosphorylate MAVS which results in recruitment of IRF3 for its phosphorylation. Furthermore, phosphorylated IRF3 subsequently forms a dimer and translocates into the nucleus to activate the IFN promoter (30).

For the Nuclear Factor Kappa-light-chain-enhancer of activated B cells(NF- κB) activation pathway, transforming growth factor-β-activated kinase 1 (TAK1) is a key player. In mammalian cells, TAK1 forms a complex with TAK1 binding proteins 1, 2, and 3 (TAB1, 2, 3), which can recruit adaptor proteins, such as TRAF6, to activate TAK1. TAK1 activation phosphorylates and activates the IKK complex (IKKβ, IKKα, and NEMO), leading to activation of NF-κB(31).

CV-A16, along with EV-A71, EV-D68 and CV-A6, is a positive-stranded RNA virus belonging to the *Picornaviridae* family. Like other members of the family, CV-A16 encodes only one single open reading frame, which can be processed into four structural (VP1, VP2, VP3, and VP4) and seven nonstructural (2A, 2B, 2C, 3A, 3B, 3C, and 3D) proteins upon viral infection(1). Among them, the EV-A71 3C protease ($3C^{pro}$) is one of the most versatile functional proteins. It possesses both proteolytic and RNA binding activities (32, 33), which enable the protease to perform multiple tasks in systems involving viral replication and pathogen-host interaction. Increasing evidence suggests that the EV-A71 $3C^{pro}$ targets innate

115 immune factors, such as RIG-I, TRIF, IRF7/9, the TAK1/TAB1/TAB2/TAB3 complex, and
116 NLRP3, to modulate type I IFN and cytokine responses(34-38). Recently, EV-D68 $3C^{pro}$ has
117 been reported to target IRF7 and TRIF to disable innate sensing responses(39, 40). However,
118 little is known about CV-A16 and CV-A6 $3C^{pro}$ function in innate immunity.

119 Here, we demonstrate that the CV-A16, CV-A6, and EV-D68 $3C^{pro}$ blocks MDA5-triggered
120 type I IFN induction. CV-A16 $3C^{pro}$ binds MDA5 and inhibits its interaction with MAVS. In
121 addition, CVA-16, CV-A6, and EV-D68 $3C^{pro}$ cleaves TAK1 to inhibit the NF- κB response.
122 Thus, our data demonstrate that circulating HFMD-associated CV-A16 and CV-A6, as well as
123 severe respiratory disease-associated EV-D68, have developed a mechanism to subvert host
124 innate immune responses by simultaneously targeting key factors in the RLR and TLR pathways.
125 These findings indicate the potential merit of targeting CV-A16, CV-A6, or EV-D68 $3C^{pro}$ as
126 anti-viral therapy.
127
128
129
130
131
132
133
134
135
136
137

MATERIALS AND METHODS

Cell lines and viruses. Human embryonic kidney 293T (HEK293T, CRL-11268) cells and human rhabdomyosarcoma RD cells (CCL-136) were purchased from ATCC and maintained in Dulbecco's modified Eagle's medium (DMEM) containing 10% heat-inactivated fetal bovine serum (FBS) (HyClone, Logan, UT), 100U/mL penicillin, and 100μg/mL streptomycin, at 37°C in a 5% CO_2 humidified atmosphere. Sendai virus (SeV) was kindly provided by Dr. Tao Wang (Tianjin University) and Dr. Junliang Chang (Jilin University).

Antibodies and reagents. The following antibodies were used for western blotting analysis in this study: anti-Flag monoclonal M2 antibody (F1804-1MG; Sigma), anti-Myc (9E10) monoclonal antibody (MMS-150P; Covance), anti-HA monoclonal antibody (MMS-101R; Covance), anti-Tubulin monoclonal antibody (MMS-410P; Covance), anti-V5 antibody (V8012, Sigma), VP1 antiserum against CA16 obtained from rabbits immunized with CA16 CC024, RIG-I (D14g6) rabbit antibody (#3743; Cell Signal), Cardif (human) antibody (AT107) (ALX-210-929-C100; Enzo Life Sciences), MDA5 (human) polyclonal antibody (AT113) (ALX-210-935-C100; Enzo Life Sciences), TAK1 antibody (2E10; NOVUS) and anti-p-IRF3 monoclonal antibody (AB76493; Abcam). Poly I:C was purchased from Guandong South China Pharmaceutical Co., LTD.

Plasmids. Flag-MAVS, V5-TBK1, Flag-IKKε, Flag-IRF3, Flag-IRF7 and firefly luciferase reporter plasmids for IFNβ were kindly provided by Dr. Tao Wang (Tianjin University). NF-κB luciferase reporter plasmid (Promega, E8491) was kindly provided by Dr. Yong Cai (College of

Life Science, Jilin University, China). Flag-TAK1 was generously gifted by Dr.Mingyu Lv (Jilin University, China). Flag-RIG-IN (CARD domain) were generously gifted by Dr. Jinhua Yang (Baylor College of Medicine, Houston, TX, US) (41). Flag-MDA5-N (1-213AA) was amplified from template (purchased from Fitgene Company, Shanghai) and cloned into the SalI and BamH I sites of VR1012 vector. Flag-IRF3-5D was constructed by Generay Biotech Co. Ltd. (Shanghai, China). Flag-TLR3 was purchased from Addgene. 3C ORFs of CV-A16 CC024 strain (Genbank #KF055238.1), EV-A71 063 strain (Genbank #HQ647172.1), CV-A6 (Changchun046/CHN/2013 7434 KT779410), and EV-D68 Fermon (AY426531.1) were cloned into VR1012-HA-Flag vector using the Sal I and BamH I sites. CV-B3 (JX312064.1) 3C expression vector was obtained from Generay Biotech Co. Ltd and the 3C containing DNA fragment was cloned into VR1012 vector using the Sal I and BamH I sites. CV-A16, EV-D68, and CV-A6 3C H40D plasmids were obtained by single site mutation.

Luciferase reporter assay. HEK293T cells were plated into 24-well dishes and transfected the following day. 100 ng of the reporter plasmid for IFN-β, NF-κB promoters, 1ng Renilla luciferase control plasmid (pRL-TK), and the indicated amounts of the expression plasmids were used per well. 24h post-transfection, cells were infected with SeV (20HA/mL) or left uninfected for 18h. Luciferase activities were then measured using a Dual-Luciferase Reporter Assay System (Promega, Madison, WI) according to the manufacturer's instructions. Firefly luciferase activity was normalized to Renilla luciferase activity. Finally, the relative luciferase activities (Rel. Lucif. Act.) were expressed as fold changes over the empty plasmids transfected or SeV non-infected controls.

184 **CPE observation.** For observing CPEs, RD cells were grown on a culture dish and infected by
185 CV-A16, CV-A6 or EV-D68 (MOI of 0.5) and treated with IFN alpha2 (1000U/mL, Changchun
186 Institute of Biological Products) separately or both at the indicated time points. Morphological
187 changes were observed and photographed under a light microscope (Olympus IX51, Tokyo,
188 Japan).
189
190 **RNA extraction and quantitative real-time PCR.** Total RNA was extracted from cells by
191 using Trizol (Invitrogen, Carlsbad, CA). Reverse transcription was carried out in a 20 μL
192 volume using a Superscript cDNA synthesis kit (Invitrogen, Carlsbad, CA) according to the
193 manufacturer's instructions. The quantitative real-time polymerase chain reaction (qPCR) was
194 carried out on an Mx3005P instrument (Agilent Technologies, Stratagene, USA) using the
195 Master Mix (SYBR Green) Kit (Bio-Rad) and primers designed using the VP1 conserved region
196 sequences of CA16 as follows: CA16-F1, CATGCAGCGCTTGTGCTT; CA16-F2,
197 CATGCAACGACTGTGCTTTC; CA16-R1, CACACAATTCCCCCGTCTTAC; CA16-R2,
198 CATAATTCGCCCGTTTTGCT. GAPDH as control: GAPDH-F:
199 CCCATCACCATCTTCCAGG; GAPDH-R: TTCTCCATGGTGGTGAAGAC. IFNB-F,
200 CACTGGCTGGAATGAGACT ; IFNB-R, TTTCGGAGGTAACCTGTAAG ; IKBA-F,
201 CGGCCTGGACTCCATGAAAG ; IKBA-R, CCTTCAC CTGGCGGATCACT ; IL-8-F,
202 CGGAAGGAACCATCTCACTGTG ; IL-8-R, AGAAATCAGGAAGGCTGCCAAG. The
203 qPCR assay was carried out in a 20 μL volume consisting of 10 μL of 2× SYBR Green Mix
204 solution, 0.4μL of 5 μmol/L of each oligonucleotide primer and 2 μL of cDNA template. The
205 target fragment amplification was carried out as follows: 50℃ for 2 min, then 95 ℃ for 10 min

followed by 50 cycles consisting of 95 ℃ for 15s and 60℃ for 1 min. The melting curve analysis was 90℃ for 1 min, then 55℃ for 30s and 95℃ for 30s.

Determination of Viral Titer. Virus titers were determined using the median end point of the cell culture's infectious dose (CCID50). Serially-diluted viruses were added to RD cells grown in 96-well plates, and 8 replicate samples were used for each dilution. CCID50 values were measured by counting infected RD cell culture wells with obvious CPEs and calculated by the Reed–Muench method(42).

Immunoprecipitation (Co-IP). After 48h transfection, cells were harvested and lysed with lysis buffer (50mM Tris-HCl, pH7.5, 150mM NaCl, 0.5% NP-40) containing a protease inhibitor cocktail (Roche, Indianapolis, IN). Lysates of cells were incubated with anti-Flag affinity matrix (Sigma A-2220) or anti-HA affinity (Roche) at 4°C overnight on a rotator. After washing with wash buffer (20mM Tris-Cl, pH7.5, 100mM NaCl, 0.05% Tween-20, 0.1mM EDTA) six times, 50μl of elution buffer (100mM Glycine-HCl, pH2.5) was added to re-suspend the beads and the eluted proteins were obtained by centrifugation, followed by SDS-PAGE and WB analysis.

Western blot analysis. Cells were harvested and lysed in RIPA lysis buffer (50mM Tris-HCl, pH7.5, 150mM NaCl, 1% NP40), and lysate was cleared by centrifugation at 16,000 g at 4°C for 5 min. Total cell extracts were subject to SDS-PAGE and transferred to nitrocellulose membranes (10401196; Whatman). After blocking with 5% nonfat dry milk in TBST for 1h at room temperature (RT), membranes were incubated with the indicated primary antibodies at 4°C overnight and then the corresponding alkaline phosphatase (AP)-conjugated secondary antibodies (Sigma) for 1h at RT. After three washes with TBST, the blots were reacted with

nitroblue tetrazolium (NBT) and 5-bromo-4-chloro-3'-indolylphosphate (BCIP) (Sigma). About endogenous TAK1, MDA5 and MAVS protein were detected by HRP-conjugated secondary antibody (Cell Signal) for 1h at RT. After three washes with TBST, the membranes were reacted with ECL sensitive kit (B500023; Proteintech) and developed by azure system c500.

Statistical analysis. Data in the luciferase reporter assay and qRT-RCR results were presented as the mean and standard error. Viral titers were analyzed using GraphPad Prism 6 software (GraphPad Software, La Jolla, CA, USA). Differences among groups were analyzed by an ANOVA test (Stata Corp, College Station, TX). P values <0.05 (significant) were considered significant.

RESULTS

Type I interferon induces potent CV-A16 inhibition. Type I IFNs are early host responses to virus infection and can induce broad anti-viral effects. Whether CV-A16 replication could be influenced by type I IFNs is not fully known. To address this question, we first treated susceptible RD cells with 1000U/mL of IFN-α2 for twelve hours. IFN-α2 treated or untreated RD cells were then infected with equal amounts of CV-A16 virus. Viral replication was monitored by the appearance of cytopathic effect (CPE) in the cell culture. In untreated RD cells, significant CPE was observed at 72 hours after infection. As expected, no CPE was observed in uninfected RD cells (Fig. 1A). IFN-α2 treatment resulted in significant viral inhibition as indicated by the reduced appearance of CPE in RD cells infected with CV-A16 (Fig. 1A). Reduced CV-A16 replication due to IFN-α2 treatment was also evaluated by monitoring viral RNA levels in infected RD cells. In IFN-α2 treated RD cells, the level of CV-A16 RNA was reduced by >90% when compared to that of virus-infected RD cells in the absence of IFN-α2 treatment (Fig. 1B).

Reduced CV-A16 virus production due to IFN-α2 treatment was also evaluated by monitoring viral titer from infected RD cells at different time points. In IFN-α2 treated RD cells, the viral titer was reduced significantly when compared to that of virus-infected RD cells in the absence of IFN-α2 treatment at different time points (Fig. 1C). These data establish that type I IFN can induce potent inhibition of CV-A16 replication.

Type I IFN treatment also resulted in significant viral inhibition of CV-A6 (Fig. 2A) and EV-D68 (Fig. 2B), as indicated by the reduced appearance of CPE in RD cells infected with

these viruses. Reduced CV-A6 (Fig. 2C) or EV-D68 (Fig. 2D) replication due to IFN-α2 treatment was also evaluated by monitoring viral titers from infected RD cells. In IFN-α2 treated RD cells, the level of CV-A6 or EV-D68 viral titer was reduced significantly at different time points when compared to that of virus-infected RD cells in the absence of IFN-α2 treatment (Fig. 2). These data establish that type I IFNs can induce potent inhibition of CV-A16, CV-A6, and EV-D68.

CV-A16, CV-A6, and EV-D68 suppress the type I IFN response triggered by RNA virus infection. It has been established that infection with the RNA virus Sendai (SeV) can stimulate the expression of interferons in mammalian cell lines (43, 44). Whether CV-A16 infection activates the innate immune system has not been widely explored. Since type I IFNs can induce potent viral inhibition, CV-A16 may have to avoid type I IFN induction during viral infection. To identify how CV-A16 affects the innate immune pathway, we first determined whether it can stimulate a type I IFN response. The IFN-β luciferase reporter(34) and an internal control pRL-TK renilla reporter (34) were co-transfected into HEK293T cells with CV-A16 or EV-A71 infectious clones or a control vector plus pT7 RNA polymerase. At 24 hours post-transfection, cells were infected with SeV or left uninfected for 18 hours. IFN-β promoter activity (as monitored by luciferase activity) was then measured. CV-A16 replication did not trigger IFN-β production (Fig. 3). As shown in Fig.3A, SeV infection stimulated IFN-β promoter activity (line 2) almost 50-fold when compared to the uninfected cells (lane 1). In contrast, CV-A16 replication in HEK293T cells showed no stimulation of the IFN-β promoter (lane 3). HEK293T cells were sensitive to CV-A16 infection, resulting in the appearance of CPE (Fig. 3C). At the same time, CV-A16 replication in HEK293T cells inhibited SeV infection-induced IFN-β

297 production (Fig. 3A, lane 4). Consistent with previous reports (35), EV-A71 replication also
298 suppressed SeV-triggered IFN-β induction (Fig.3A, lane 6).

299 In addition to activating type I IFN pathways, RNA virus infection can also trigger NF-κB
300 activation. We examined NF-κB promoter activity after SeV infection in the absence or presence
301 of CV-A16 or EV-A71. EV-A71 barely activated the NF-κB promoter, which is consistent with
302 previous reports (35, 36, 45). Moreover, we revealed that CV-A16 did not trigger NF-κB
303 activation. Similar to their effects on the suppression of IFN-β production, SeV-mediated NF-κB
304 promoter activation was significantly suppressed by CV-A16 and EV-A71 (Fig. 3B, compare
305 lanes 2, 4 and 6). These results indicate that host immune defense systems are impaired during
306 CV-A16 virus propagation. We have also observed that CV-A6 or EV-D68 virus infection did
307 not trigger type I IFN (Fig. 3D) or NF-κB (Fig. 3E) production. Furthermore, SeV-mediated type
308 I IFN (Fig. 3D) and NF-κB (Fig. 3E) production was significantly suppressed by CV-A6 or EV-
309 D68 infection. Enterovirus 2Apro cleaves eukaryotic initiation factors 4GI and 4GII (eIF4GI
310 and eIF4GII) within virus-infected cells(46-48). CV-A16 2A protease could inhibit SeV
311 replication by inhibiting cap-dependent mRNA translation and inhibiting SeV-induced activation
312 of MAVS signaling. It is thus important to address whether CV-A16 3Cpro expression alone
313 could suppression of SeV triggered immune activation.
314
315 **3C^{pro} of CV-A16 suppresses SeV induced type I IFN response.** In addition to its role in
316 viral polyprotein processing, 3C^{pro} of certain enteroviruses has been shown to play a pivotal role
317 in suppressing IFN-β production(35-38, 49-53). However, the role of 3C^{pro} of CV-A16, CV-A6
318 and EV-D68 in suppressing IFN-β activation has not been well characterized. To determine the
319 capacity of CV-A16 3C^{pro} to block the type I IFN response, IFN-β promoter activity in the

absence or presence of CV-A16 $3C^{pro}$ was assessed using the luciferase assay. As shown in Fig. 4A, expression of CV-A16 $3C^{pro}$ inhibited SeV-induced IFN-β promoter activity significantly. As expected, similar activity for EV-A71 $3C^{pro}$ was observed (Fig. 4A) when both proteins were expressed at similar levels (Fig. 4B). Thus, our results indicate that CV-A16 utilizes $3C^{pro}$ to antagonize type I IFN induction. Consistent with the IFN-β promoter assay results, endogenous IFN-β mRNA expression was induced by SeV infection and was then reduced in a dose dependent manner by the addition of CV-A16 $3C^{pro}$ (Fig. 4C). Type I IFN-induced ISG56 mRNA expression was also induced by SeV infection and was then similarly inhibited by the addition of CV-A16 $3C^{pro}$ (Fig. 4C).

In response to RNA virus infection, the cytosolic RNA sensors RIG-I and MDA5 initiate antiviral signaling, and consequently a number of downstream molecules are recruited and activated (18). IFN-β transcription and production requires IRF3 phosphorylation and dimerization after virus stimulation. To further confirm the inhibitory effect of CV-A16 $3C^{pro}$ on type I IFN responses, we assayed for IRF3 phosphorylation. Plasmids encoding CV-A16 $3C^{pro}$ or EV-A71 $3C^{pro}$ were co-transfected into HEK293T cells with an IRF3 expression vector for 24 hours. Transfected cells were then treated with SeV for another 24 hours, followed by western blot analysis for phosphorylated IRF3. IRF3 phosphorylation could be triggered by SeV infection (Fig. 4D, lane 4). However, IRF3 phosphorylation was inhibited significantly in cells expressing CV-A16 $3C^{pro}$ or EV-A71 $3C^{pro}$ (Fig. 4D, lanes 5 and 6). The $2A^{pro}$ of EV-A71 has also been reported to inhibit innate immune responses (38, 45, 54-58). We have observed that CV-A16 $2A^{pro}$ could enhance the CV-A16 $3C^{pro}$-mediated type I IFN activation inhibition induced after SeV infection (Fig. 4E).

342 We have also observed that CV-A6 or EV-D68 $3C^{pro}$ inhibited SeV-induced IFN-β promoter
343 activation (Fig. 4F). SeV infection-triggered IRF3 phosphorylation was also inhibited
344 significantly in cells expressing CV-A6 $3C^{pro}$ or EV-D68 $3C^{pro}$ (Fig. 4G). Collectively, our
345 results demonstrate that $3C^{pro}$ of CV-A16, CV-A6, and EV-D68 are all able to inhibit type I IFN
346 responses.

347 **$3C^{pro}$ of CV-A16, CV-A6, or EV-D68 inhibits type I IFN responses upstream of IRF3**
348 **activation**. Since CV-A16 $3C^{pro}$ expression inhibited IRF3 phosphorylation, we first determined
349 whether CV-A16 $3C^{pro}$ can directly influence the function of IRF3. To address this question, a
350 constitutively active form of IRF3 (IRF3-5D(44)) was used to induce the activation of the IFN-β
351 promoter in HEK293T cells transfected with IRF3-5D alone or co-transfected with CV-A16
352 $3C^{pro}$. Consistent with a previous report (37), ectopic expression of IRF3-5D stimulated IFN-β
353 induction (Fig. 5A). IFN-β activation stimulated by IRF3-5D was not inhibited by CV-A16 $3C^{pro}$
354 (Fig. 5A). CV-A16 $3C^{pro}$ protein expression was confirmed by western blot analysis (Fig. 5B).
355 IFN-β promoter activation stimulated by IRF3-5D was also not inhibited by CV-A6 or EV-D68
356 $3C^{pro}$ (Fig. 5A). IKKε (Fig. 5C) and TBK1 (Fig. 5D) also stimulated IFN-β expression, which
357 was consistent with previously reports (35, 59, 60). None of CV-A16, CV-A6, or EV-D68 $3C^{pro}$
358 had an inhibitory effect on IFN-β promoter activation induced by IKKε (Fig. 5C) or TBK1
359 (Fig.5C). Collectively, our results have demonstrated that $3C^{pro}$ of CV-A16, CV-A6, or EV-D68
360 inhibits the induction of type I IFN responses upstream of IRF3, TBK1, and IKKε.

361 **CA16 $3C^{pro}$ neutralizes MDA5-mediated type I IFN activation.** Upon virus infection, MDA5
362 binds viral RNA and interacts with the adaptor protein, MAVS. This interaction leads to the
363 activation of downstream factors (TRAFs, TBK1, etc.). These activated factors cause IRF3 to
364 dimerize and then translocate into the nucleus, inducing an IFN-β response. Therefore, using

previously established experimental strategies (61), we asked whether CV-A16 $3C^{pro}$ could target MDA5 and impair its immune activation functionalities. In contrast to type I IFN activation by IRF3, TBK1, and IKKε, which is resistant to CV-A16 $3C^{pro}$, we observed that type I IFN activation induced by MDA5-N (35, 62) was inhibited by CV-A16 $3C^{pro}$ (Fig. 6A). A CV-A16 $3C^{pro}$ catalytic site mutant (H40D) could still inhibit MDA5-N-induced IFN activation (Fig. 6A). The MDA5-N protein level was not down-regulated in the presence of CV-A16 $3C^{pro}$ (Fig. 6B). Endogenous MDA5 (Fig. 6C) and MAVS (Fig. 6D) expression was also not affected by CV-A16 $3C^{pro}$. It has been reported that EV-A71 and EV-D68 $3C^{pro}$ could induce the cleavage of IRF7 (37, 39). We did not detect cleaved IRF7 product in the presence of CV-A16 $3C^{pro}$ (Fig. 6E).

We next examined whether CV-A16 $3C^{pro}$ has the ability to interact with MDA5. A Co-immunoprecipitation (Co-IP) assay was performed as previously described (63) to evaluate whether MDA5 associates with CV-A16 $3C^{pro}$. As shown in Fig. 6F, CV-A16 $3C^{pro}$ (HA-tagged) was immunoprecipitated with both the Myc-tagged MDA5 (lane 7) and MDA5-N (lane 9). In the absence of Myc-tagged MDA5 or MDA5-N, CV-A16 $3C^{pro}$ was not detected (Fig. 6F, lane 6), indicating the specificity of the assay system. CV-A16 $3C^{pro}$ (H40D) interaction with MDA5 (Fig. 6F, lane 8) or MDA5-N (lane 10) was also observed.

Although the CV-A16 $3C^{pro}$ catalytic site mutant (H40D) could still interact with MDA5, mutations of surface exposed residues (Fig. 7A) of the N-terminal region of CV-A16 $3C^{pro}$ disrupted its interaction with MDA5 (Fig. 7B). CV-A16 $3C^{pro}$M also had impaired ability to inhibit MDA5-N-induced type I IFN activation (Fig. 7C). MDA5 interaction with CV-A16 $3C^{pro}$ was not disrupted by RNase treatment (Fig. 7D). CV-A16 $3C^{pro}$ V154S containing a mutation of the C-terminal residue involved in RNA binding (33) also maintained the ability to inhibit MDA5-N-induced type I IFN activation (Fig. 7E).

388 MDA5 binds viral RNA and interacts with the adaptor protein MAVS to trigger immune
389 activation. Next, we asked whether CV-A16 $3C^{pro}$ can impair MAVS association with MDA5.
390 To answer this question, we carried out a Co-IP assay. HEK293T cells were transfected with
391 vectors expressing Flag-MAVS along with Myc-MDA5-N, CV-A16 3C-HA, or a control vector.
392 At 48 hours after transfection, cells were lysed and incubated with anti-Flag beads, followed by
393 analysis with a western blot. As expected, MAVS interacted with MDA5-N (Fig. 8A, lane 8). In
394 the absence of MAVS, MDA5-N was not detected (Fig. 8A, lane 6), indicating the specificity of
395 the assay. The results additionally showed that the association of MAVS and MDA5-N was
396 disrupted by $3C^{pro}$ in a dose dependent manner (Fig. 8A, lanes 9, 10 and Fig.8B). Immune
397 activation triggered by MDA5-N was also disrupted by CV-A16 $3C^{pro}$ in a dose dependent
398 manner (Fig. 8C). CV-A16 infection could inhibit MDA5 interaction with endogenous MAVS
399 (Fig. 8D). Interestingly, MDA5 dimerization was also inhibited by CV-A16 $3C^{pro}$ (Fig. 8E).
400 Dimerization of MDA5 has been reported to be important for MDA5 interaction with MAVS
401 (62, 64, 65).
402 Upon RNA virus infection, the RIG-I-like receptors RIG-I and MDA5 detect viral RNA
403 through their CTD domains. The CARD domains of RIG-I and MDA5 are responsible for
404 transducing signals to the downstream adaptor MAVS through CARD-CARD interactions(61,
405 62, 66, 67).To investigate whether CV-A16 $3C^{pro}$ also antagonizes RIG-I-induced MAVS
406 activation in the RLR pathway, we performed an IFN-β luciferase assay in HEK293T cells. A
407 RIG-IN expression vector, which includes the caspase recruitment domain, was employed (66,
408 68). As illustrated in Fig. 9A, CV-A16 $3C^{pro}$ could significantly suppress RIG-IN-mediated IFN-
409 β activation in a dose dependent manner. Expression of $3C^{pro}$ impaired the interaction between
410 MAVS and RIG-IN (Fig. 9B). In addition, the RIG-IN protein level was not down-regulated in

411 the presence of $3C^{pro}$. The association of MAVS and RIG-IN was disrupted by CV-A16 $3C^{pro}$ in
412 a dose dependent manner (Figs. 9B and C).

413 CV-A16 $3C^{pro}$ interacted with both RIG-I (Fig. 10B) and RIG-IN (Fig. 10B). Its interaction
414 with RIG-I was not impaired by RNase treatment (Fig. 10C). Like wild-type CV-A16 $3C^{pro}$, the
415 CV-A16 $3C^{pro}$ H40D mutant maintained the ability to inhibit RIG-IN-triggered immune
416 activation (Fig. 10A) and could still interact with RIG-I (Fig. 10B, lane 8) and RIG-IN (Fig. 10B,
417 lane 10). Also, the H40D mutant could still inhibit RIG-IN interaction with MAVS (Fig. 10D),
418 similar to its ability to inhibit MDA5-N interaction with MAVS (Fig. 10E). Together, these
419 results indicate that CV-A16 $3C^{pro}$ targets MDA5 and RIG-I, culminating in inactivation of the
420 IFN-β induction pathway. $3C^{pro}$ failed to block IFN-β activation mediated by TBK1 and
421 downstream factors (Fig. 5C). This finding indicates that $3C^{pro}$ probably acts upstream of TBK1
422 in the RIG-I-RLR pathway and that RIG-I, like MDA5, is a target of $3C^{pro}$.

423 **$3C^{pro}$ from EV-D68 and CV-A6 neutralizes MDA5-mediated type I IFN activation.** Direct
424 targeting of MDA5 by the *Picornaviridae* family of viruses has not been widely reported
425 previously. To further investigate whether 3C proteases from other enterovirus species also
426 possess the ability to interact with MDA5 and affect its function, the expression vectors for EV-
427 A71, EV-D68, CV-A6, and CV-B3 $3C^{pro}$ were constructed and compared. Interaction of $3C^{pro}$
428 with MDA5-N was first examined by Co-IP experiments. The Co-IP results (Fig.11A) indicated
429 that, similar to those for CV-A16 $3C^{pro}$, $3C^{pro}$ from EV-D68 and CV-A6 also interacted with
430 MDA5-N. At the same time, EV-A71 and CV-B3 $3C^{pro}$ interacted with MDA5-N poorly (Fig.
431 11A).

432 The level of MDA5-N was lower in the presence of EV-D68 and CV-A6 $3C^{pro}$ (Fig.11A).
433 To determine whether this was due to the protease activity of these $3C^{pro}$, we constructed CV-A6

434 and EV-D68 3C protease active site mutants (H40D). The reduced levels of MDA5-N were still
435 noted with these mutants when compared to the controls (Figs. 11B and C). Thus, it is unlikely
436 that the reduced levels of MDA5-N by CV-A6 and EV-D68 $3C^{pro}$ are due to protease digestion.
437 Future studies will be required to determine the mechanism of MDA5 reduction by CV-A6 and
438 EV-D68 $3C^{pro}$. However, despite lower levels of MDA5-N in the presence of CV-A6 and EV-
439 D68 $3C^{pro}$ (Fig. 11A, lanes 5 and 6) when compared to the control sample (Fig. 11A, lane 1), co-
440 IP of MDA5-N with CV-A6 and EV-D68 $3C^{pro}$ was still detected (Fig. 11A, lanes 11 and 12) but
441 not in the control sample (lane 7).

442 To address the question of whether $3C^{pro}$ from EV-D68 and CV-A63C^{pro} could also
443 antagonize MDA5-mediated IFN-β activation, we performed an IFN-β luciferase assay in
444 HEK293T cells. CV-A6 (Fig. 11D) and EV-D68 (Fig. 11E) $3C^{pro}$ efficiently suppressed MDA5-
445 N-induced IFN-β promoter activity. Collectively, our data suggest that disabling MDA5 and
446 MAVS interaction through the activity of 3C proteases may be a common strategy used by a
447 variety of enterovirus species.

448 **$3C^{pro}$ from CV-A16, CV-A6, and EV-D68 targets TAK1 to impair SeV-triggered NF-κB**
449 **response.** As indicated in Fig. 2B, CV-A16 virus can also block NF-κB activation after SeV
450 infection. In fact, CV-A16 $3C^{pro}$ alone can potently suppress NF-κB activation after SeV
451 infection (Fig. 12A, lanes 3 and 4). Endogenous NF-κB-activated IKB (Fig. 12B) and IL-8 (Fig.
452 12C) mRNA levels were also suppressed by CV-A16 $3C^{pro}$ after SeV infection. Several studies
453 have demonstrated that TAK1 is a key player in NF-κB activation ((34, 69)). In response to
454 interleukin-1, tumor necrosis factor-α, and toll-like receptor agonists, it mediates the activation
455 of NF-κB, c-Jun N-terminal kinase (JNK), and p38 pathways (69). In order to assess whether
456 TAK1 is the target of CV–A16 $3C^{pro}$ in the NF-κB pathway, we examined TAK1 expression and

processing in the presence or absence of $3C^{pro}$ in HEK293T cells. TAK1 was transfected with different amounts of the $3C^{pro}$ expression vector, and protein expression was detected by western blot. Interestingly, TAK1 cleavage products were induced by CV-A16 $3C^{pro}$ expression (Fig. 12D, lanes 2 and 3) compared with the control (Fig. 12D, lane 1). A TAK1-related smaller protein band around 45KD was detected in the presence of CV-A16 $3C^{pro}$. To further evaluate whether $3C^{pro}$-induced TAK1 cleavage is protease activity dependent, we examined CV-A16 $3C^{pro}$ H40D versus wild type $3C^{pro}$. As shown in Fig. 12D (lanes 4 and 5), the appearance of the cleaved TAK1 fragment was not detected in the presence of the CV-A16 $3C^{pro}$ H40D mutant. Thus, the protease activity of CV-A16 $3C^{pro}$ is required for TAK1 cleavage. At the same time, the ability of the $3C^{pro}$ H40D mutant to suppress NF-κB activation after SeV infection was also impaired (Fig. 12A, lanes 5 and 6). The ability to cleave TAK1 was also observed for the $3C^{pro}$ from EV-D68 (Fig. 12F) and CV-A6 (Fig. 12G). Similarly, the $3C^{pro}$ from EV-D68 and CV-A6 suppressed NF-κB activation after SeV infection (Fig. 12E).

$3C^{pro}$ from CV-A16, CV-A6, and EV-D68 inhibits TLR3-mediated NF-κB response. In addition to the RLR pathway, TLR3 detection of the RNA component of RNA viruses also triggers NF-κB activation. Ectopic expression of TLR3 in HEK293T cells led to NF-κB activation in the presence of poly I:C (Fig. 13A, lane 2). CV-A16 $3C^{pro}$ suppressed TLR3-triggered NF-κB activation (Fig. 13A, lane 3). In contrast, the ability of the CV-A16 $3C^{pro}$ H40D mutant to suppress TLR3-triggered NF-κB activation was impaired (Fig. 13A, lane 4). Cleavage of endogenous TAK1 could be detected in the presence of CV-A16 $3C^{pro}$ (Fig. 13B). CV-A16 infection could also trigger TAK cleavage (Fig. 13C). The $3C^{pro}$ from EV-D68 and CV-A6 also suppressed TLR3-triggered NF-κB activation (Fig. 13D). CV-A6 $3C^{pro}$ H40D (Fig. 13E) or EV-

D68 $3C^{pro}$ H40D (Fig. 13F) mutants were not able to cleave TAK1, unlike wild-type $3C^{pro}$. These mutants also had impaired ability to suppress TLR3-triggered NF-κB activation (Fig. 13D).

DISCUSSION

In this study, we evaluated the role of $3C^{pro}$ in viral evasion of host innate immune responses for several poorly studied enteroviruses and coxsackieviruses, including CV-A16, CV-A6, and EV-D68. In a systematic evaluation, we observed that CV-A16, CV-A6, and EV-D68 $3C^{pro}$ could block immune activation triggered by the RNA virus SeV (Fig. 4). Furthermore, CV-A16, CV-A6, and EV-D68 $3C^{pro}$ inhibited IRF3 phosphorylation after SeV infection (Fig. 4). At the same time, CV-A16, CV-A6, and EV-D68 $3C^{pro}$ did not block type I IFN activation induced by TBK1 or IKKε downstream factors (Fig. 5). Instead, CV-A16 (Fig. 6), CV-A6, and EV-D68 (Fig. 10) $3C^{pro}$ directly interferes with MDA5-MAVS functional signaling.

CV-A16 $3C^{pro}$ impaired MDA5-CARD-induced IFN-β activation in a dose dependent manner (Fig. 6). CV-A16 $3C^{pro}$ binds to MDA5 (Fig. 6) and disrupts its interaction with MAVS (Fig. 8). In a manner distinct from other RNA viruses (51, 54), CV-A16 $3C^{pro}$ suppressed MDA5-triggered type I IFN activation without reducing MDA5 (Fig. 6C) or MAVS expression (Fig. 6D). The interaction between CV-A16 $3C^{pro}$ and MDA5 was not affected by RNase treatment (Fig. 7). Mutation of the protease active site of CV-A16 $3C^{pro}$ also did not abolish its interaction with MDA5 (Fig. 6). On the other hand, mutations of N-terminal surface exposed amino acids inhibited its interaction with MDA5 (Fig. 7). To our knowledge, this is the first example that the 3C protein of the *Picornaviridae* family of viruses interfering with MDA5-MAVS interaction to abrogate type I IFN induction.

The ability to interact with MDA5 was also evaluated for various enteroviruses and coxsackieviruses linked to HFMD and pediatric respiratory disease. We observed the interaction between MDA5 and the $3C^{pro}$ from CV-A6 and EV-D68 (Fig. 11). Like CV-A16, $3C^{pro}$ from

525 CV-A6 and EV-D68 could efficiently antagonize MDA5-induced IFN-β activation (Fig. 11). On
526 the other hand, we did not detect an interaction between $3C^{pro}$ from CV-B3 or EV-A71 and
527 MDA5 (Fig. 11).Whether disruption of MDA5 function by the $3C^{pro}$ is seen among other diverse
528 *Picornaviridae* is a question that requires further investigation.

529 MDA5 is a critical component in the host RLR pathway. Several studies using $MDA5^{-/-}$
530 knockout mice have demonstrated that MDA5 signaling is critical for type-I IFN induction after
531 virus infection (70, 71). MDA5-deficient mice have increased susceptibility to lethal infection
532 induced by poliovirus (70, 71). It is interesting to note that EV-A71 $3C^{pro}$ has been reported not
533 to interfere with MDA5-mediated IFN restriction (35). These results are consistent with our
534 observation that EV-A71 $3C^{pro}$ did not interact with MDA5 (Fig. 11). It is possible that EV-A71
535 and CV-B3 3C proteases use different strategies to neutralize IFN-β activation mediated by
536 MDA5. For instance, CV-B3 3C protein targets MAVS (49) and EV-A71 3C protein targets IRF7
537 (35) in the RLR pathway to impair MDA5 induced IFNβ activation.

538 In addition to type I IFN activation, SeV infection also triggers NF-kB activation through
539 TAK1. We have demonstrated that TAK1 was also targeted by CV-A16 $3C^{pro}$ (Fig. 12). CV-A16
540 $3C^{pro}$ expression resulted in TAK1 cleavage, and this function was blocked by a CV-A16 $3C^{pro}$
541 active site (H40D) mutation (Fig. 12). Consequently, NF-kB activation triggered by SeV
542 infection was inhibited by CV-A16 $3C^{pro}$ but not the mutant $3C^{pro}$ H40D (Fig. 12). We also
543 observed both CV-A6 and EV-D68 $3C^{pro}$ harbor the same ability to diminish NF-κB signal by
544 targeting TAK1 (Fig. 12). The protease active site was also important for CV-A6 and EV-D68
545 $3C^{pro}$ to diminish NF-κB signal by cleaving TAK1 (Fig. 12).

546 Apart from the RLR pathway, TLRs are also critical for detecting the RNA component of
547 RNA viruses. Among them, TLR3 is one of the essential TLRs for sensing invading viral RNA.

548 TLR3 can activate TAK1 and subsequently stimulate p38, JNK and NF-κB signals leading to
549 cytokine production. TLR3-triggered NF-κB activation was inhibited by CV-A16, CV-A6, or
550 EV-D68 $3C^{pro}$ but not their H40D mutants (Fig. 13). The cleaved fragment of TAK1 was around
551 45KD. As a result, the integrity of TAK1 functional domains was destroyed. The N-terminal
552 fragment of TAK1 includes the TAB1 binding and kinase domains which are critical for TAK1
553 activation. The C-terminal fragment of TAK1 includes the TAB2/3 binding domain which is
554 necessary for the activation of downstream IKK kinase (IKKβ, IKKα). Thus, the separation of
555 the N-terminal and C-terminal domains of TAK1 by CV-A16, CV-A6, or EV-D68 $3C^{pro}$ will lead
556 to the disruption of host RLR and TLR pathways. In addition to innate immune responses, TAK1
557 plays a central role in host adaptive immunity. T cell receptor (TCR) ligation leads to TAK1-
558 mediated activation of both NF-kB and JNK, which is required for the development and
559 maturation of T cells. CV-A16 has been shown to infect T cells (72). In light of impaired NF-kB
560 activation by $3C^{pro}$ targeting TAK1, CV-A16 may interfere with T cell activation and maturation
561 *in vivo*. The interplay between CV-A16 infection and adaptive immunity should be studied in the
562 future.

563 During virus infection, host cells utilize different strategies to combat virus invasion.
564 Viruses have also evolved sophisticated mechanisms to subvert host immune responses. Overall,
565 we showed in this study that $3C^{pro}$ proteins of CV-A16, CV-A6, and EV-D68 utilize novel tactics
566 to subvert host innate immune responses by targeting key factors in the RLR and TLR pathways.
567 This information should contribute to our understanding of the pathogenesis of CV-A16, CV-A6,
568 and EV-D68 infection. Furthermore, recognition of the critical role of this protease in the
569 pathogenesis of CV-A16, CV-A6, and EV-D68 infection and the success of protease inhibitors in

the treatment of other viral infections provides a foundation for development of new therapeutic agents to treat HFMD and pediatric respiratory disease.

ACKNOWLEDGMENTS

We thank ChunyanDai, Xin Liu, and Zhaolong Li for technical assistance, Tao Wang and Jinhua Yang for critical reagents. This work was supported in part by funding from the Chinese Ministry of Science and Technology (number 2012CB911100 and number 2013ZX0001-005) and the Chinese Ministry of Education (number IRT1016), the Key Laboratory of Molecular Virology, Jilin Province (20102209), the China Scholarship Council to Yajuan Rui (201406170086).

Author contributions: Xiao-Fang Yu designed the overall project. Yajuan Rui, Jiaming Su, Hong Wang, and Junliang Chang performed the experiments and Xiao-Fang Yu, Richard Markham, Shaohua Wang, Yong Cai, Wenwen Zheng, Wenyan Zhang, James T. Gordy, Wei Wei, and Wei Kong analyzed the data. Xiao-Fang Yu, James T. Gordy, Richard Markham, and Yajuan Rui wrote the paper with help from other authors.

REFERENCES

1. **McMinn PC.** 2002. An overview of the evolution of enterovirus 71 and its clinical and public health significance. FEMS microbiology reviews **26:**91-107.
2. **Qiu J.** 2008. Enterovirus 71 infection: a new threat to global public health? The Lancet. Neurology **7:**868-869.
3. **Bendig JW, Fleming DM.** 1996. Epidemiological, virological, and clinical features of an epidemic of hand, foot, and mouth disease in England and Wales. Communicable disease report. CDR review **6:**R81-86.
4. **Yen FB, Chang LY, Kao CL, Lee PI, Chen CM, Lee CY, Shao PL, Wang SC, Lu CY, Huang LM.** 2009. Coxsackieviruses infection in northern Taiwan--epidemiology and clinical characteristics. Journal of microbiology, immunology, and infection = Wei mian yu gan ran za zhi **42:**38-46.
5. **Wang CY, Li Lu F, Wu MH, Lee CY, Huang LM.** 2004. Fatal coxsackievirus A16 infection. The Pediatric infectious disease journal **23:**275-276.
6. **Wright HT, Jr., Landing BH, Lennette EH, Mc AR.** 1963. Fatal infection in an infant associated with Coxsackie virus group A, type 16. The New England journal of medicine **268:**1041-1044.
7. 2014. Enterovirus D68: the unexpected guest. Lancet Infectious Diseases **14:**1023-1023.
8. **Brown BA, Nix WA, Sheth M, Frace M, Oberste MS.** 2014. Seven Strains of Enterovirus D68 Detected in the United States during the 2014 Severe Respiratory Disease Outbreak. Genome Announcements **2**.
9. **Selvarangan R, Gerber SI, Midgley CM, Jackson MA, Turabelidze G, Obringer E, Johnson D, Giles BL, Patel A, Echols F.** 2014. Severe Respiratory Illness Associated with Enterovirus D68—Missouri and Illinois, 2014. American Journal of Transplantation Official Journal of the American Society of Transplantation & the American Society of Transplant Surgeons **14:**2662-2663.
10. **Nelson R.** 2014. Outbreaks of enterovirus D68 continue across the USA. Lancet Respiratory Medicine **2:**791-791.
11. **Messacar K, Schreiner TL, Maloney JA, Wallace A, Ludke J, Oberste MS, Nix WA, Robinson CC, Glodé MP, Abzug MJ.** 2015. A cluster of acute flaccid paralysis and cranial nerve dysfunction temporally associated with an outbreak of enterovirus D68 in children in Colorado, USA. Lancet **385:**1662-1671.
12. **Oermann CM, Schuster JE, Conners GP, Newland JG, Selvarangan R, Jackson MA.** 2015. Enterovirus D68. A Focused Review and Clinical Highlights from the 2014 U.S. Outbreak. Ann Am Thorac Soc **12**.
13. **Sinclair C, Gaunt E, Simmonds P, Broomfield D, Nwafor N, Wellington L, Templeton K, Willocks L, Schofield O, Harvala H.** 2014. Atypical hand, foot, and mouth disease associated with coxsackievirus A6 infection, Edinburgh, United Kingdom, January to February 2014. Euro surveillance : bulletin Europeen sur les maladies transmissibles = European communicable disease bulletin **19:**20745.
14. **Chong JH, Aan MK.** 2014. An atypical dermatologic presentation of a child with hand, foot and mouth disease caused by coxsackievirus A6. The Pediatric infectious disease journal **33:**889.
15. **Downing C, Ramirez-Fort MK, Doan HQ, Benoist F, Oberste MS, Khan F, Tyring SK.** 2014. Coxsackievirus A6 associated hand, foot and mouth disease in adults: clinical presentation and review of the literature. Journal of clinical virology : the official publication of the Pan American Society for Clinical Virology **60:**381-386.
16. **Ben-Chetrit E, Wiener-Well Y, Shulman LM, Cohen MJ, Elinav H, Sofer D, Feldman I, Marva E, Wolf DG.** 2014. Coxsackievirus A6-related hand foot and mouth disease: skin manifestations in a cluster of adult patients. Journal of clinical virology : the official publication of the Pan American Society for Clinical Virology **59:**201-203.
17. **Feder HM, Jr., Bennett N, Modlin JF.** 2014. Atypical hand, foot, and mouth disease: a vesiculobullous eruption caused by Coxsackie virus A6. The Lancet. Infectious diseases **14:**83-86.
18. **Kawai T, Akira S.** 2006. Innate immune recognition of viral infection. Nature immunology **7:**131-137.
19. **Takeuchi O, Akira S.** 2007. Recognition of viruses by innate immunity. Immunological reviews **220:**214-224.
20. **Wu J, Chen ZJ.** 2014. Innate immune sensing and signaling of cytosolic nucleic acids. Annual review of immunology **32:**461-488.
21. **Hornung V, Ellegast J, Kim S, Brzozka K, Jung A, Kato H, Poeck H, Akira S, Conzelmann KK, Schlee M, Endres S, Hartmann G.** 2006. 5'-Triphosphate RNA is the ligand for RIG-I. Science **314:**994-997.

22. **Pichlmair A, Schulz O, Tan CP, Naslund TI, Liljestrom P, Weber F, Reis e Sousa C.** 2006. RIG-I-mediated antiviral responses to single-stranded RNA bearing 5'-phosphates. Science **314:**997-1001.
23. **Reikine S, Nguyen JB, Modis Y.** 2014. Pattern Recognition and Signaling Mechanisms of RIG-I and MDA5. Frontiers in immunology **5:**342.
24. **Feng Q, Langereis MA, Olagnier D, Chiang C, van de Winkel R, van Essen P, Zoll J, Hiscott J, van Kuppeveld FJ.** 2014. Coxsackievirus cloverleaf RNA containing a 5' triphosphate triggers an antiviral response via RIG-I activation. PloS one **9:**e95927.
25. **Feng Q, Hato SV, Langereis MA, Zoll J, Virgen-Slane R, Peisley A, Hur S, Semler BL, van Rij RP, van Kuppeveld FJ.** 2012. MDA5 detects the double-stranded RNA replicative form in picornavirus-infected cells. Cell reports **2:**1187-1196.
26. **Takahasi K, Kumeta H, Tsuduki N, Narita R, Shigemoto T, Hirai R, Yoneyama M, Horiuchi M, Ogura K, Fujita T, Inagaki F.** 2009. Solution structures of cytosolic RNA sensor MDA5 and LGP2 C-terminal domains: identification of the RNA recognition loop in RIG-I-like receptors. The Journal of biological chemistry **284:**17465-17474.
27. **Kawai T, Takahashi K, Sato S, Coban C, Kumar H, Kato H, Ishii KJ, Takeuchi O, Akira S.** 2005. IPS-1, an adaptor triggering RIG-I- and Mda5-mediated type I interferon induction. Nature immunology **6:**981-988.
28. **Meylan E, Curran J, Hofmann K, Moradpour D, Binder M, Bartenschlager R, Tschopp J.** 2005. Cardif is an adaptor protein in the RIG-I antiviral pathway and is targeted by hepatitis C virus. Nature **437:**1167-1172.
29. **Seth RB, Sun L, Ea CK, Chen ZJ.** 2005. Identification and characterization of MAVS, a mitochondrial antiviral signaling protein that activates NF-kappaB and IRF 3. Cell **122:**669-682.
30. **Liu S, Cai X, Wu J, Cong Q, Chen X, Li T, Du F, Ren J, Wu YT, Grishin NV, Chen ZJ.** 2015. Phosphorylation of innate immune adaptor proteins MAVS, STING, and TRIF induces IRF3 activation. Science **347:**aaa2630.
31. **Hayden MS, Ghosh S.** 2008. Shared principles in NF-kappaB signaling. Cell **132:**344-362.
32. **Li ML, Hsu TA, Chen TC, Chang SC, Lee JC, Chen CC, Stollar V, Shih SR.** 2002. The 3C protease activity of enterovirus 71 induces human neural cell apoptosis. Virology **293:**386-395.
33. **Shih SR, Chiang C, Chen TC, Wu CN, Hsu JT, Lee JC, Hwang MJ, Li ML, Chen GW, Ho MS.** 2004. Mutations at KFRDI and VGK domains of enterovirus 71 3C protease affect its RNA binding and proteolytic activities. Journal of biomedical science **11:**239-248.
34. **Lei X, Han N, Xiao X, Jin Q, He B, Wang J.** 2014. Enterovirus 71 3C inhibits cytokine expression through cleavage of the TAK1/TAB1/TAB2/TAB3 complex. Journal of virology **88:**9830-9841.
35. **Lei X, Liu X, Ma Y, Sun Z, Yang Y, Jin Q, He B, Wang J.** 2010. The 3C protein of enterovirus 71 inhibits retinoid acid-inducible gene I-mediated interferon regulatory factor 3 activation and type I interferon responses. Journal of virology **84:**8051-8061.
36. **Lei X, Sun Z, Liu X, Jin Q, He B, Wang J.** 2011. Cleavage of the adaptor protein TRIF by enterovirus 71 3C inhibits antiviral responses mediated by Toll-like receptor 3. Journal of virology **85:**8811-8818.
37. **Lei X, Xiao X, Xue Q, Jin Q, He B, Wang J.** 2013. Cleavage of interferon regulatory factor 7 by enterovirus 71 3C suppresses cellular responses. Journal of virology **87:**1690-1698.
38. **Wang H, Lei X, Xiao X, Yang C, Lu W, Huang Z, Leng Q, Jin Q, He B, Meng G, Wang J.** 2015. Reciprocal Regulation between Enterovirus 71 and the NLRP3 Inflammasome. Cell reports **12:**42-48.
39. **Xiang Z, Liu L, Lei X, Zhou Z, He B, Wang J.** 2016. 3C Protease of Enterovirus D68 Inhibits Cellular Defense Mediated by Interferon Regulatory Factor 7. Journal of virology **90:**1613-1621.
40. **Xiang Z, Li L, Lei X, Zhou H, Zhou Z, He B, Wang J.** 2014. Enterovirus 68 3C protease cleaves TRIF to attenuate antiviral responses mediated by Toll-like receptor 3. Journal of virology **88:**6650-6659.
41. **Fan Y, Mao R, Yu Y, Liu S, Shi Z, Cheng J, Zhang H, An L, Zhao Y, Xu X, Chen Z, Kogiso M, Zhang D, Zhang H, Zhang P, Jung JU, Li X, Xu G, Yang J.** 2014. USP21 negatively regulates antiviral response by acting as a RIG-I deubiquitinase. The Journal of experimental medicine **211:**313-328.
42. **Reed LJ, Muench H.** 1938. A SIMPLE METHOD OF ESTIMATING FIFTY PER CENT ENDPOINTS. American Journal of Epidemiology **27**.
43. **Strahle L, Garcin D, Le Mercier P, Schlaak JF, Kolakofsky D.** 2003. Sendai virus targets inflammatory responses, as well as the interferon-induced antiviral state, in a multifaceted manner. Journal of virology **77:**7903-7913.

44. **Lin R, Heylbroeck C, Pitha PM, Hiscott J.** 1998. Virus-dependent phosphorylation of the IRF-3 transcription factor regulates nuclear translocation, transactivation potential, and proteasome-mediated degradation. Molecular and cellular biology **18:**2986-2996.
45. **Lu J, Yi L, Zhao J, Yu J, Chen Y, Lin MC, Kung HF, He ML.** 2012. Enterovirus 71 disrupts interferon signaling by reducing the level of interferon receptor 1. Journal of virology **86:**3767-3776.
46. **Kräusslich HG, Nicklin MJ, Toyoda H, Etchison D, Wimmer E.** 1987. Poliovirus proteinase 2A induces cleavage of eucaryotic initiation factor 4F polypeptide p220. Journal of virology **61:**2711-2718.
47. **Liebig HD, Seipelt J, Vassilieva E, Gradi A, Kuechler E.** 2002. A thermosensitive mutant of HRV2 2A proteinase: evidence for direct cleavage of eIF4GI and eIF4GII. Febs Letters **523:**53-57.
48. **Liebig HD, Ziegler E, Yan R, Hartmuth K, Klump H, Kowalski H, Blaas D, Sommergruber W, Frasel L, Lamphear B, et al.** 1993. Purification of two picornaviral 2A proteinases: interaction with eIF-4 gamma and influence on in vitro translation. Biochemistry **32:**7581-7588.
49. **Mukherjee A, Morosky SA, Delorme-Axford E, Dybdahl-Sissoko N, Oberste MS, Wang T, Coyne CB.** 2011. The coxsackievirus B 3C protease cleaves MAVS and TRIF to attenuate host type I interferon and apoptotic signaling. PLoS pathogens **7:**e1001311.
50. **Barral PM, Sarkar D, Fisher PB, Racaniello VR.** 2009. RIG-I is cleaved during picornavirus infection. Virology **391:**171-176.
51. **Barral PM, Morrison JM, Drahos J, Gupta P, Sarkar D, Fisher PB, Racaniello VR.** 2007. MDA-5 is cleaved in poliovirus-infected cells. Journal of virology **81:**3677-3684.
52. **Papon L, Oteiza A, Imaizumi T, Kato H, Brocchi E, Lawson TG, Akira S, Mechti N.** 2009. The viral RNA recognition sensor RIG-I is degraded during encephalomyocarditis virus (EMCV) infection. Virology **393:**311-318.
53. **Huang L, Liu Q, Zhang L, Zhang Q, Hu L, Li C, Wang S, Li J, Zhang Y, Yu H, Wang Y, Zhong Z, Xiong T, Xia X, Wang X, Yu L, Deng G, Cai X, Cui S, Weng C.** 2015. Encephalomyocarditis Virus 3C Protease Relieves TRAF Family Member-associated NF-kappaB Activator (TANK) Inhibitory Effect on TRAF6-mediated NF-kappaB Signaling through Cleavage of TANK. The Journal of biological chemistry **290:**27618-27632.
54. **Feng Q, Langereis MA, Lork M, Nguyen M, Hato SV, Lanke K, Emdad L, Bhoopathi P, Fisher PB, Lloyd RE, van Kuppeveld FJ.** 2014. Enterovirus 2Apro targets MDA5 and MAVS in infected cells. Journal of virology **88:**3369-3378.
55. **Wang B, Xi X, Lei X, Zhang X, Cui S, Wang J, Jin Q, Zhao Z.** 2013. Enterovirus 71 protease 2Apro targets MAVS to inhibit anti-viral type I interferon responses. PLoS pathogens **9:**e1003231.
56. **Wang LC, Chen SO, Chang SP, Lee YP, Yu CK, Chen CL, Tseng PC, Hsieh CY, Chen SH.** 2015. Enterovirus 71 Proteins 2A and 3D Antagonize the Antiviral Activity of Gamma Interferon via Signaling Attenuation. **89:**7028-7037.
57. **Liu Y, Zhang Z, Zhao X, Yu R, Zhang X, Wu S, Liu J, Chi X, Song X, Fu L, Yu Y, Hou L, Chen W.** 2014. Enterovirus 71 inhibits cellular type I interferon signaling by downregulating JAK1 protein expression. Viral immunology **27:**267-276.
58. **Lei X, Xiao X, Wang J.** 2016. Innate Immunity Evasion by Enteroviruses: Insights into Virus-Host Interaction. Viruses **8**.
59. **Fitzgerald KA, McWhirter SM, Faia KL, Rowe DC, Latz E, Golenbock DT, Coyle AJ, Liao SM, Maniatis T.** 2003. IKKepsilon and TBK1 are essential components of the IRF3 signaling pathway. Nature immunology **4:**491-496.
60. **Sharma S, tenOever BR, Grandvaux N, Zhou GP, Lin R, Hiscott J.** 2003. Triggering the interferon antiviral response through an IKK-related pathway. Science **300:**1148-1151.
61. **Xu L, Xiao N, Liu F, Ren H, Gu J.** 2009. Inhibition of RIG-I and MDA5-dependent antiviral response by gC1qR at mitochondria. Proceedings of the National Academy of Sciences of the United States of America **106:**1530-1535.
62. **Jiang X, Kinch LN, Brautigam CA, Chen X, Du F, Grishin NV, Chen ZJ.** 2012. Ubiquitin-induced oligomerization of the RNA sensors RIG-I and MDA5 activates antiviral innate immune response. Immunity **36:**959-973.
63. **Zhang W, Du J, Evans SL, Yu Y, Yu XF.** 2012. T-cell differentiation factor CBF-beta regulates HIV-1 Vif-mediated evasion of host restriction. Nature **481:**376-379.

64. **Berke IC, Modis Y.** 2012. MDA5 cooperatively forms dimers and ATP-sensitive filaments upon binding double-stranded RNA. The EMBO journal **31:**1714-1726.
65. **Hou F, Sun L, Zheng H, Skaug B, Jiang QX, Chen ZJ.** 2011. MAVS forms functional prion-like aggregates to activate and propagate antiviral innate immune response. Cell **146:**448-461.
66. **Gack MU, Shin YC, Joo CH, Urano T, Liang C, Sun L, Takeuchi O, Akira S, Chen Z, Inoue S, Jung JU.** 2007. TRIM25 RING-finger E3 ubiquitin ligase is essential for RIG-I-mediated antiviral activity. Nature **446:**916-920.
67. **Pham AM, Santa Maria FG, Lahiri T, Friedman E, Marie IJ, Levy DE.** 2016. PKR Transduces MDA5-Dependent Signals for Type I IFN Induction. PLoS pathogens **12:**e1005489.
68. **Wang S, Wang K, Lin R, Zheng C.** 2013. Herpes simplex virus 1 serine/threonine kinase US3 hyperphosphorylates IRF3 and inhibits beta interferon production. Journal of virology **87:**12814-12827.
69. **Dai L, Aye Thu C, Liu XY, Xi J, Cheung PC.** 2012. TAK1, more than just innate immunity. IUBMB life **64:**825-834.
70. **Abe Y, Fujii K, Nagata N, Takeuchi O, Akira S, Oshiumi H, Matsumoto M, Seya T, Koike S.** 2012. The toll-like receptor 3-mediated antiviral response is important for protection against poliovirus infection in poliovirus receptor transgenic mice. Journal of virology **86:**185-194.
71. **Wang JP, Cerny A, Asher DR, Kurt-Jones EA, Bronson RT, Finberg RW.** 2010. MDA5 and MAVS mediate type I interferon responses to coxsackie B virus. Journal of virology **84:**254-260.
72. **Nishimura Y, Shimojima M, Tano Y, Miyamura T, Wakita T, Shimizu H.** 2009. Human P-selectin glycoprotein ligand-1 is a functional receptor for enterovirus 71. Nature medicine **15:**794-797.

779 **FIGURE LEGENDS**

780

781 Figure 1. Type I interferon induces potent CV-A16 inhibition. (A) RD cells were untreated
782 (columns 1, 3) or treated with 1000U/mL of interferon α2 (columns 2, 4). After 12 hours, IFN-α2
783 treated or untreated RD cells were infected with equal amounts (MOI of 0.5) of CV-A16 virus
784 (columns 3, 4) or left uninfected (columns 1, 2). 72 hours later, cells were observed for
785 morphological changes and were photographed by light microscopy at 400X magnification. (B)
786 Total viral RNA was extracted from the treated RD cells listed above (Figure1A). The viral RNA
787 levels of CV-A16 were evaluated by real-time PCR using SYBR green. Primers targeted CV-
788 A16 VP1 to monitor viral replication. GAPDH expression was used as a control. Data represent
789 the average of three independent experiments. The error bars indicate the SD of three
790 independent experiments. P values <0.05 were considered significant. (C) CV-A16 virus from
791 RD cells were collected at days 0, 1, 2, 3, and 4 after infection with or without IFN-α2 treatment.
792 The virus titer was determined by CCID50.

793

794 Figure 2. Type I interferon induces potent CV-A6 and EV-D68 inhibition. (A) RD cells were
795 untreated (column 1) or treated with 1000U/mL of interferon α2 (column 2). After 12 hours,
796 IFN-α2 treated or untreated RD cells were infected with equal amounts (MOI of 0.5) of CV-A6
797 virus or EV-D68 virus (B). 96 hours later, cells were observed for morphological changes and
798 photographed by light microscopy at 400X magnification. CV-A16 virus (C) or EV-D68 virus
799 (D) from RD cells were collected at days 0, 1, 2, 3, and 4 after infection with or without IFN-α2
800 treatment. The virus titer was determined by CCID50.

801

802 Figure 3. CV-A16, CV-A6, and EV-D68 suppress the type I IFN response triggered by RNA
803 virus infection. HEK293T cells were transfected with the pRL-TK plasmid and the IFN-β (A) or
804 NF- κB promoter (B) plus control plasmids or CV-A16 or EV-A71 infectious clone vectors for
805 24 hours. The cells were subsequently infected with SeV (20HA/mL) or left uninfected for 20
806 hours, and then cell lysates were assayed for luciferase activity. Data represent the average of
807 three independent experiments. The error bars indicate the SD of three replicates within one
808 experiment. P values <0.05 were considered significant. (C) HEK293T cells were infected with
809 CV-A16 virus (MOI of 0.5) or left uninfected. After the indicated time points, cells were
810 observed for CPE. HEK293T cells were transfected with the pRL-TK plasmid and the IFN-β (D)
811 or NF- κB promoter (E) for 12 hours and were then infected with CV-A6 and EV-D68 virus
812 (MOI of 0.5) for 12 hours. The cells were subsequently infected with SeV (20HA/mL) or left
813 uninfected for 20 hours, and then cell lysates were assayed for luciferase activity. Data represent
814 the average of three independent experiments. The error bars indicate the SD of three replicates
815 within one experiment. P values <0.05 were considered significant.
816
817 Figure 4. $3C^{pro}$ of CV-A16, CV-A6, and EV-D68 suppresses the SeV-induced type I IFN
818 response. HEK293T cells were transfected with empty vector, CV-A16 3C, or EV-A71 3C (A),
819 or with empty vector, CV-A6 3C, or EV-D68 3C (F), along with the pRL-TK plasmid and the
820 IFN-β reporter. After 24 hours, cells were challenged with SeV (20HA/mL) or left uninfected for
821 20 hours and were followed for luciferase activity. Protein expression was detected by western
822 blot (B). Data represent the average of three independent experiments. The error bars indicate the
823 SD of three replicates within one experiment. P values <0.05 were considered significant. (C)
824 HEK293T cells were transfected with empty vector, 150ng CV-A16 3C, and 450ng CV-A16 3C.

825 After 24 hours, cells were challenged with SeV (20HA/mL) or left uninfected for 20 hours. Then
826 the cells were harvested, and RNA was extracted to determine *IFNB* and *ISG56* mRNA level by
827 quantitative real-time PCR. (D) HEK293T cells were transfected with the Flag-IRF3 plasmid
828 alone (lane 1), Flag-CV-A16 3C alone (lane 2), Flag-EV-A71 3C alone (lane 3), Flag-IRF3 plus
829 Flag-CV-A16 3C (lane 5), or Flag-IRF3 plus Flag-EV-A71 3C (lane 6). 24 hours after the
830 transfection, cells were treated with SeV (SeV+; 20HA/mL) or were left untreated (SeV-). 24
831 hours later, cells were analyzed by western blot with antibodies against Flag-IRF3, p-IRF3, Flag-
832 3C, or tubulin control. (E) HEK293T cells were transfected with 200ng CV-A16 2A (lane 3),
833 CV-A16 3C at two doses (150ng, 450ng) (lanes 4, 5), or 200ng 2A with 3C at two doses (150ng,
834 450ng) (lanes 6, 7). 24 hours after the transfection, cells were treated with SeV (SeV+;
835 20HA/mL) or were left untreated (SeV-). 24 hours later, cell lysates were assayed for luciferase
836 activity. (G) HEK293T cells were transfected with the Flag-IRF3 plasmid alone (lanes 1, 4) or in
837 combination with HA-EV-D68 3C (lanes 2, 5) or HA-CV-A6 3C (lanes 3, 6). 24 hours after the
838 transfection, cells were treated with SeV (SeV+; 20HA/mL) or were left untreated (SeV-). 24
839 hours later, cells were analyzed by western blot with antibodies against Flag-IRF3, p-IRF3, HA-
840 3C, or tubulin control.
841
842 Figure 5. $3C^{pro}$ of CV-A16, CV-A6, and EV-D68 inhibits type I interferon responses upstream of
843 IRF3 activation. HEK293T cells were transfected with IFNβ-luc and IRF3-5D(A), IKKε(C) or
844 TBK1 (D) together with control (pRL-TK), CV-A16 3C, CV-A6 3C, or EV-D68 3C expression
845 vectors. 36 hours after transfection, cells were assayed for luciferase activity. Data are
846 representative of three independent experiments. The error bars indicate the SD of three different
847 experiments. P values <0.05 were considered significant. (B) CV-A16, CV-A6, and EV-D68 3C

848 protein expression was analyzed by western blot with HA antibody. Tubulin antibody was used
849 as a control.
850
851 Figure 6. CA16 $3C^{pro}$ neutralizes MDA5-mediated IFN-β activation. (A) HEK293T cells were
852 transfected with the pRL-TK plasmid and IFN-β-luc promoter reporter plus control plasmid (lane
853 1), Flag-MDA5-N alone (lane 2), Flag-MDA5-N plus three increasing doses of CV-A16 3C
854 (lanes 3-5), or Flag-MDA5-N plus three increasing doses of CV-A16 3C H40D (lanes 6-8). After
855 a 36 hour transfection, cells were assayed for luciferase activity and then analyzed by western
856 blot. Proteins were detected with the indicated antibodies. Tubulin antibody was used as a
857 control (B). Data are a representative of three independent experiments with triplicate samples.
858 The error bars indicated the SD of three different experiments. P values <0.05 were considered
859 significant. (C) HEK293T cells were transfected with two increasing doses of CV-A16 3C
860 plasmids (lanes 2, 3) or control vector (lane 1). 36 hours later, cells were harvested, and 3C-HA
861 along with endogenous MDA5 (C) or MAVS (D) proteins were analyzed by western blot.
862 Tubulin antibody was used as a control. (E) HEK293T cells were transfected with IRF7-Flag and
863 two increasing doses of CV-A16 3C dose or negative control. 36 hours later, proteins were
864 detected with the indicated antibodies by western blot. (F) HEK293T cells were co-transfected
865 with Myc-MDA5 (lanes 2, 3) or Myc-MDA5-N (lanes 4, 5), and with control vector (lane 1),
866 HA-CV-A16 3C (lanes 2, 4), or with HA-CV-A16 3C H40D (lanes 3, 5). 48 hours after
867 transfection, cell lysates were immunoprecipitated with anti-Myc beads. Western blot was used
868 to analyze protein expression.

869 Figure 7. The N-terminal domain of CV-A16 is critical for its function. (A) Here is a schematic
870 of CV-A16's N-terminal amino acids and the designed mutant. (B) HEK293T cells were

transfected with MDA5-N-Myc and HA-CV-A16 3C (lane 2) or its mutant HA-CV-A16 3C-M (lane 3). At 48 hours after transfection, cells were harvested and cell lysates were incubated with anti-HA beads overnight. Protein expression was detected by the indicated antibodies by western blot. Tubulin antibody was used as a control. (C) HEK293T cells were transfected with the pRL-TK plasmid and IFNβ-luc promoter reporter plus control plasmid (lane 1), MDA5-N-Myc (lanes 2-7), or different amounts of HA-3C (lanes 3-5) or HA-3C-M (lanes 6, 7) expression vectors. 36 hours after transfection, cell lysates were assayed for luciferase activity. Data are a representative of three independent experiments. (D) HEK293T cells were transfected with MDA5-Myc and HA-CV-A16 3C (lanes 2, 3) or HA-CV-A16 3C alone (lane 1). At 48 hours after transfection, cells were harvested, and cell lysates were treated with RNase (lane 3) or left untreated (lanes 1, 2) and incubated with anti-Myc beads overnight. Protein expression was detected by western blot using the indicated antibodies. Tubulin antibody was used as a control. (E) HEK293T cells were transfected with pRL-TK plasmid and IFNβ-luc promoter reporter plus control plasmid (lane 1), MDA5-N-Myc alone (lane 2) or cotransfected with different amounts of HA-3C (lanes 3-5) or HA-3C V154S (lanes 6-8) expression vectors. 36 hours after transfection, cell lysates were assayed for luciferase activity. Data are a representative of three independent experiments. The error bars indicate the SD of three different experiments. P values <0.05 were considered significant.

Figure 8. CV-A16 3C disrupts MAVS and MDA5-N interaction. (A) HEK293T cells were transfected with plasmids encoding MDA5-N-Myc (lanes 1,3,4,5), MAVS-Flag (lanes 2–5), HA-3C (lanes 1,2,4,5) or control vector (lanes 1–3). At 48 hours after transfection, cells were harvested, and cell lysates were incubated with anti-Flag beads overnight. Protein expression was detected by western blot utilizing the indicated antibodies. Tubulin antibody was used as a

894 control. (B) ImageJ software (NIH) was used to quantitate protein band intensities, and the value
895 of MDA5-N that co-precipitated with MAVS in the absence of 3C was set to 1. A representative
896 of three independent experiments is shown in this figure. (C) HEK293T cells were transfected
897 with pRL-TK plasmid and IFN-β-luc promoter reporter plus control plasmid (lane 1), MDA5-N-
898 Myc (lanes 3-6), or different amounts (50ng,150ng,450ng) of HA-3C (lanes 2, 4-6) expression
899 vector. 36 hours after transfection, cell lysates were assayed for luciferase activity. Data are a
900 representative of three independent experiments. The error bars indicate the SD of three different
901 experiments. P values <0.05 were considered significant. (D) HEK293T cells were transfected
902 with MDA5-N-Flag or were left untreated for 12 hours and then were infected with an increasing
903 MOI (2,3) of CV-A16 virus or left untreated. 20 hours later, cells were harvested, and cell lysates
904 were incubated with anti-Flag beads overnight. Protein expression was detected by western blot
905 using the indicated antibodies. Tubulin antibody was used as a control. (E) HEK293T cells were
906 transfected with plasmids encoding MDA5-N-Myc (lanes 1, 3, 4), MDA5-N-Flag (lanes 2–4),
907 HA-3C (lanes 1, 2, 4), or control vector (lanes 1–3). At 48 hours after transfection, cells were
908 harvested and cell lysates were incubated with anti-Flag beads overnight. Protein expression was
909 detected by western blot using the indicated antibodies. Tubulin antibody was used as a control.
910
911 Figure 9. CV-A16 $3C^{pro}$ disrupts the MAVS and RIG-IN complex. (A) HEK293T cells were
912 transfected with the pRL-TK plasmid and IFN-β-luc promoter reporter plus control plasmid (lane
913 1), RIG-IN-Myc (lanes 3-6) or different amounts of HA-3C (lanes 2, 4-6) expression vectors. At
914 36 hours after transfection, cell lysates were assayed for luciferase activity. Data are
915 representative of three independent experiments. The error bars indicate the SD of three different
916 experiments. P values <0.05 were considered significant. (B) HEK293T cells were transfected

with plasmids encoding RIG-IN-Myc (lanes 1, 3–5), MAVS-Flag (lanes 2–5), HA-3C (lanes 1, 2, 4, 5), or control vector (lanes 1–3). 48 hours after transfection, cells were harvested, lysed, and then incubated with anti-Flag beads overnight. Protein expression was analyzed by western blot using the indicated antibodies. Tubulin antibody was used as a control. (C) ImageJ software (NIH) was used to quantitate protein band intensities, and the value of RIG-IN co-precipitated with MAVS in the absence of 3C was set to 1. A representative of three independent experiments is shown in this figure.

Figure 10. CV-A16 $3C^{pro}$ disruption of the MAVS and RIG-IN complex is independent of protease activity. (A) HEK293T cells were transfected with the pRL-TK plasmid and IFN-β-luc promoter reporter plus control plasmid (lane 1), RIG-IN-Myc (lane 2) alone or cotransfected with different amounts of HA-3C (lanes 3-5) or HA-3C H40D (lanes 6-8) expression vectors. At 36 hours after transfection, cell lysates were assayed for luciferase activity. Protein expression was detected by western blot using indicated antibodies. Data are representative of three independent experiments. The error bars indicate the SD of three different experiments. P values <0.05 were considered significant. (B) HEK293T cells were transfected with RIG-I-Flag (lanes 2, 3) or RIG-IN-Flag (lanes 4, 5) in combination with control vector, HA-CV-A16 3C (lanes 2, 4), or with HA-CV-A16 3C H40D (lanes 3, 5). 48 hours after transfection, cell lysates were immunoprecipitated with anti-Flag beads. Western blot was used to analyze protein expression. (C) HEK293T cells were transfected with RIG-I-Flag and HA-CV-A16 3C (lanes 2, 3) or HA-CV-A16 3C alone (lane 1). At 48 hours after transfection, cells were harvested, and cell lysates were treated with RNase (lane 3) or were left untreated (lane 2). Cell lysates were then incubated with anti-Flag beads overnight. Protein expression was detected by western blot using the

940 indicated antibodies. Tubulin antibody was used as a control. (D) HEK293T cells were
941 transfected with plasmids encoding RIG-IN-Myc with MAVS-Flag (lanes 2-5), HA-3C H40D
942 (lanes 1, 3, 4, 5) or control vector (lane 2). 48 hours after transfection, cells were harvested,
943 lysed, and then incubated with anti-Flag beads overnight. Protein expression was analyzed by
944 western blot using the indicated antibodies. Tubulin antibody was used as a control. (E)
945 HEK293T cells were transfected with plasmids encoding MDA5-N-Myc with MAVS-Flag
946 (lanes 2-5), HA-3C H40D (lanes 1, 3, 4, 5), or control vector (lane 2). 48 hours after transfection,
947 cells were harvested, lysed, and then incubated with anti-Flag beads overnight. Protein
948 expression was analyzed by western blot using the indicated antibodies. Tubulin antibody was
949 used as a control.
950
951 Figure 11. $3C^{pro}$ from CV-A6 and EV-D68 neutralizes MDA5-mediated IFN-β activation, and
952 enterovirus 3C proteases selectively associate with MDA5-N. (A) HEK 293T cells were
953 transfected with plasmids encoding MDA5-N-Myc and HA-3C (lanes 2-6) from different species
954 of enterovirus or control vector (lane 1). At 48 hours after transfection, cells were harvested,
955 lysed, and then incubated with anti-HA beads overnight. Protein expression was analyzed by
956 western blot using the indicated antibodies. Tubulin antibody was used as a control. (B)
957 HEK293T cells were transfected with GFP, MDA5-N-Flag, and control vector (lane 1), CV-A6
958 3C (lane 2) or CV-A6 3C H40D (lane 3). 36 hours later, cells were harvested and analyzed by
959 western blot. (C) HEK293T cells were transfected with GFP, MDA5-N-Flag, and control vector
960 (lane 1), EV-D68 3C (lane 2) or EV-D68 3C H40D (lane 3). 36 hours later, cells were harvested
961 and analyzed by western blot. (D) HEK293T cells were transfected with pRL-TK plasmid and
962 IFNβ-luc promoter reporter plus control plasmid (lane 1), MDA5-N-Myc (lanes 2-3) or CV-A6

963 3C (lane 3) expression vectors. At 36 hours after transfection, cell lysates were assayed for
964 luciferase activity. Data are representative of three independent experiments. The error bars
965 indicate the SD of three different experiments. (E) pRL-TK plasmid and IFNβ-luc promoter
966 reporter were transfected with control plasmid (lane 1), MDA5-N-Myc (lanes 2-3), or EV-D68
967 3C (lane 3) expression vectors into HEK293T cells. At 36 hours after transfection, cell lysates
968 were assayed for luciferase activity. Data are representative of three independent experiments.
969 The error bars indicate the SD of three different experiments.
970
971 Figure 12. $3C^{pro}$ from CA16, CV-A6, and EV-D68 targets TAK1 to impair the NF- κB response.
972 (A) HEK293T cells were transfected with pRL-TK plasmid and NF- κB -luc promoter reporter
973 plus control plasmid (lane 1), HA-CV-A16 3C (lanes 3, 4), or HA-3C H40D (lanes 5, 6). At 24
974 hours after transfection, cells were challenged with SeV (20HA/mL). 24 hours later, cell lysates
975 were assayed for luciferase activity. Data are representative of three independent experiments.
976 The error bars indicated the SD of three different experiments. P values <0.05 were considered
977 significant. (B) HEK293T cells were transfected with empty vector or increasing amounts of
978 CV-A16 3C expression vector. After 24 hours, cells were challenged with SeV (20HA/mL) or
979 left uninfected for 20 hours. Then the cells were harvested and RNA was extracted to determine
980 *IKBA* (B) and *IL-8* (C) mRNA level by quantitative real-time PCR. (D) HEK293T cells were
981 transfected with plasmids encoding TAK1-Flag and control vector (lane 1), different amounts
982 (150ng, 450ng) of HA-3C (lanes 2, 3) or HA-3C H40D (lanes 4, 5). 36 hours later, lysates of
983 cells were analyzed by western blot with antibodies against Flag and tubulin. Tubulin antibody
984 was used as a control. (E) HEK293T cells were transfected with pRL-TK plasmid and NF- κB -
985 luc promoter reporter plus control plasmid (lane 1), CV-A6 3C (lane 3) or EV-D68 3C (lane 4).

24 hours after transfection, cells were challenged with SeV (20HA/mL). 24 hours later, cell lysates were assayed for luciferase activity. Data are representative of three independent experiments. The error bars indicate the SD of three different experiments. P values <0.05 were considered significant. (F) HEK293T cells were transfected with plasmids encoding TAK1-Flag and control vector (lane 1), EV-D68 3C (lanes 2) or CV-A6 3C (G) (lane 2). 36 hours later, lysates of cells were analyzed by western blot with antibodies against Flag and tubulin. Tubulin antibody was used as a control.

Figure 13. CV-A16, CV-A6, or EV-D68 3Cpro inhibits the TLR3-mediated NF-κB response. (A) HEK293T cells were transfected with pRL-TK plasmid, NF- κB -luc promoter reporter and Flag-TLR3 expression vector alone or with CV-A16 3C or CV-A16 3C H40D. 24 hours later, cells were treated with poly I:C for 12 hours, and then cell lysates were analyzed by luciferase activity. Data are representative of three independent experiments. The error bars indicated the SD of three different experiments. (B) HEK293T cells were transfected with the TAK1-Flag expression vector. 12 hours later, cells were treated with increasing MOI (2,3) of CV-A16 virus for 20 hours. Then cell lysates were analyzed by western blot. (C) HEK293T cells were transfected with different amount of HA-CV-A16 3C plasmids (lanes 2, 3) or control vector (lane 1). 36 hours later, cells were harvested and endogenous TAK1 and 3C-HA protein were analyzed by western blot. Tubulin antibody was used as a control. (D) HEK293T cells were transfected with pRL-TK plasmid, NF- κB -luc promoter reporter and Flag-TLR3 expression vector alone or along with CV-A6 3C or EV-D68 3C or their protease mutation H40D. 24 hours later, cells were treated with poly I:C for 12 hours, then cell lysates were analyzed by luciferase activity. Data are representative of three independent experiments. The error bars indicated the

SD of three different experiments. TAK1-Flag was transfected with CV-A6 3C or its mutation H40D(E), or with EV-D68 3C or its mutation H40D (F). 36 hours later, cells were harvested and proteins were analyzed by western blot. Tubulin antibody was used as a control.

Figure 14. Summary of the sites of CV-A16 $3C^{pro}$ activity in suppressing type I IFN and NF-κB pathways. The RNA virus enters target cells through the endocytic pathway, and TLRs detect the viral genomes in endosomes. Then, TLRs engage the cytosolic adapter to activate the E3 ubiquitin (Ub) ligase, TRAF6, which ubiquitinates itself and recruits TAB proteins. TAB proteins activate TAK1. As a result, the IKK complex (IKKβ, IKKα, and NEMO) is activated, which phosphorylates IκB proteins. Phosphorylation of IκB leads to its ubiquitination and proteasomal degradation, freeing NF-κB. Active NF-κB translocates to the nucleus to induce inflammatory cytokine production. Once in the cytoplasm, viral RNA can be detected by RIG-I/MDA5 which activates the IFN-β induction pathway through MAVS, located on mitochondria. In our model, CV-A16, CV-A6, and EV-D68$3C^{pro}$ all target TAK1 and also disrupt the association of MDA5 and MAVS.

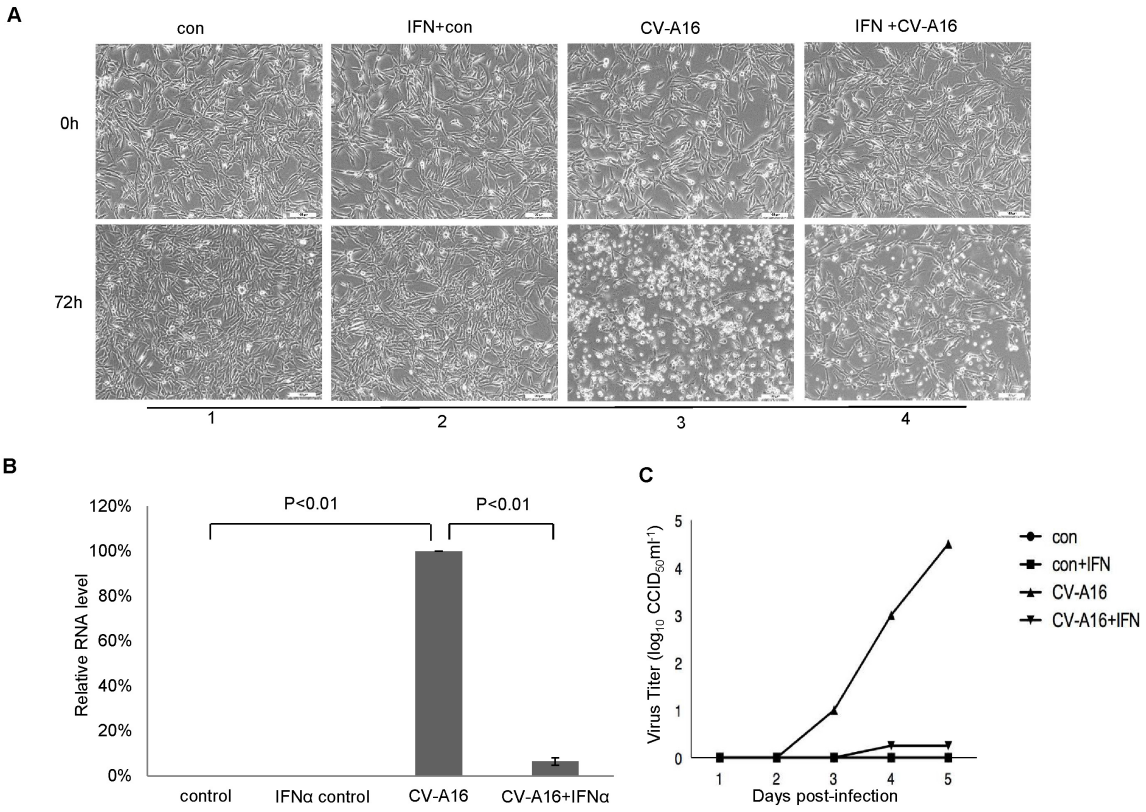

Fig. 1

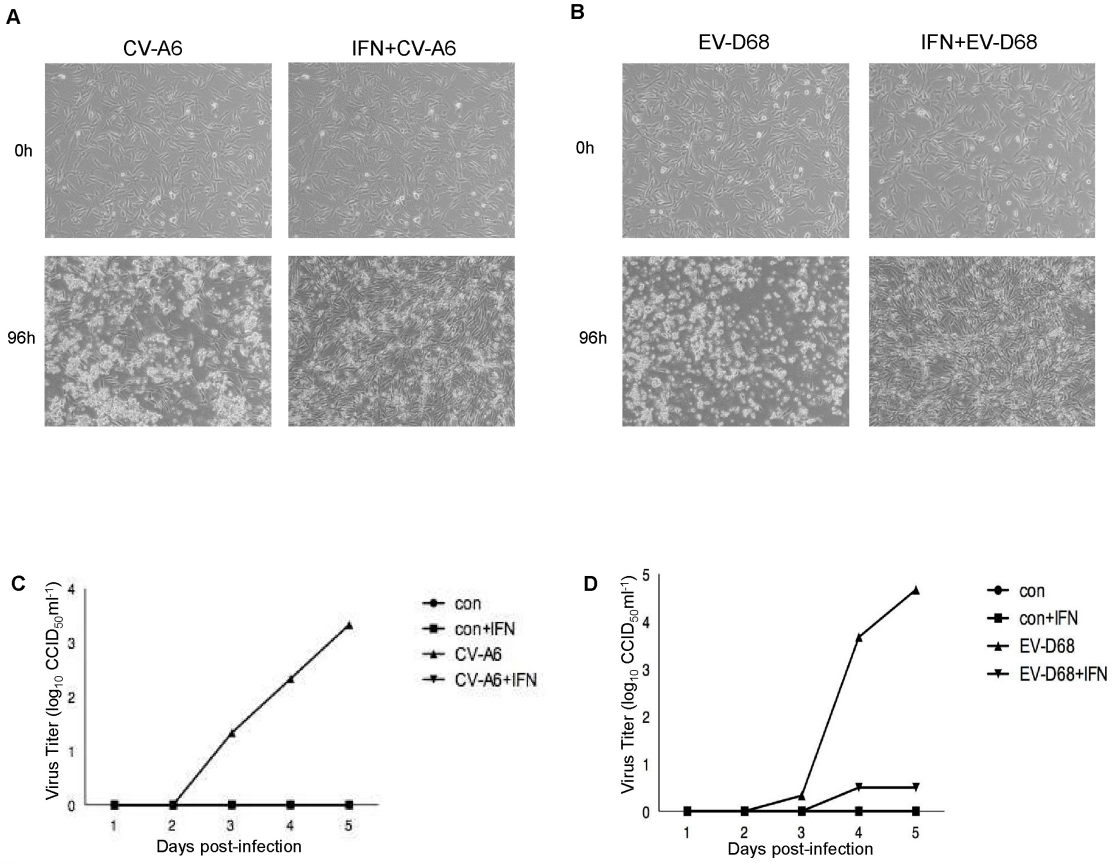

Fig. 2

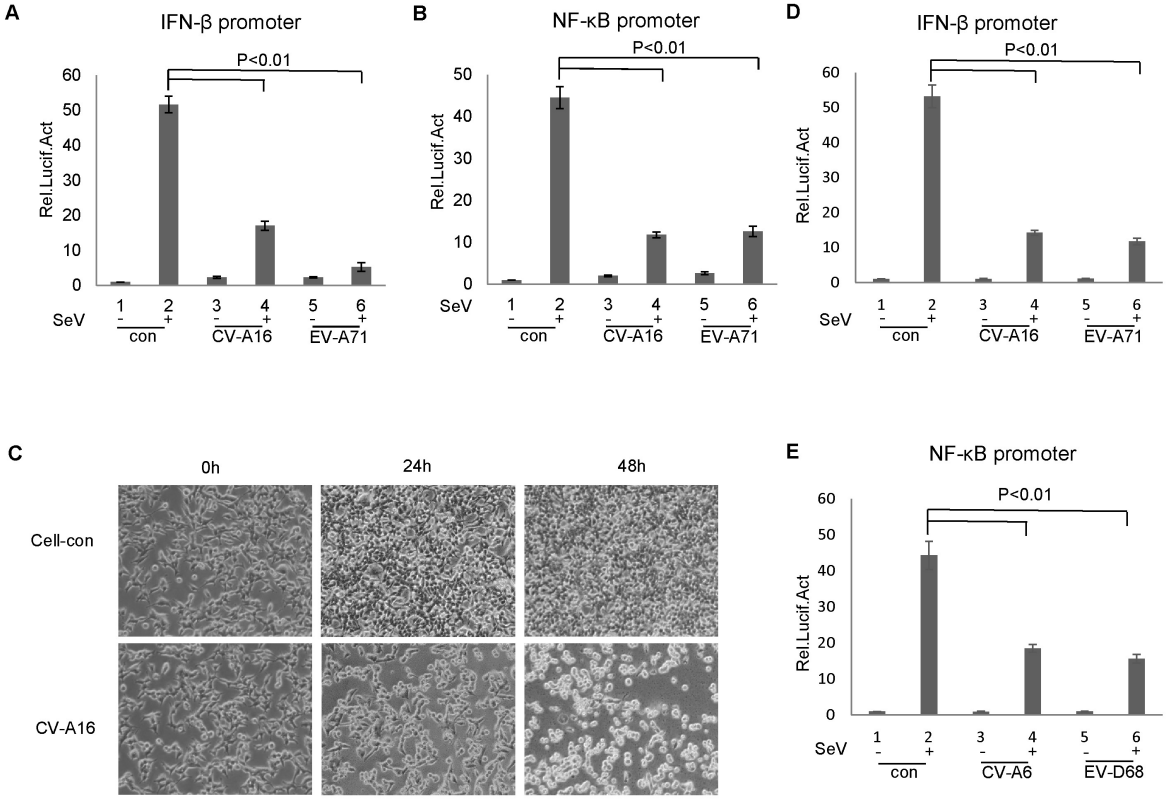

Fig. 3

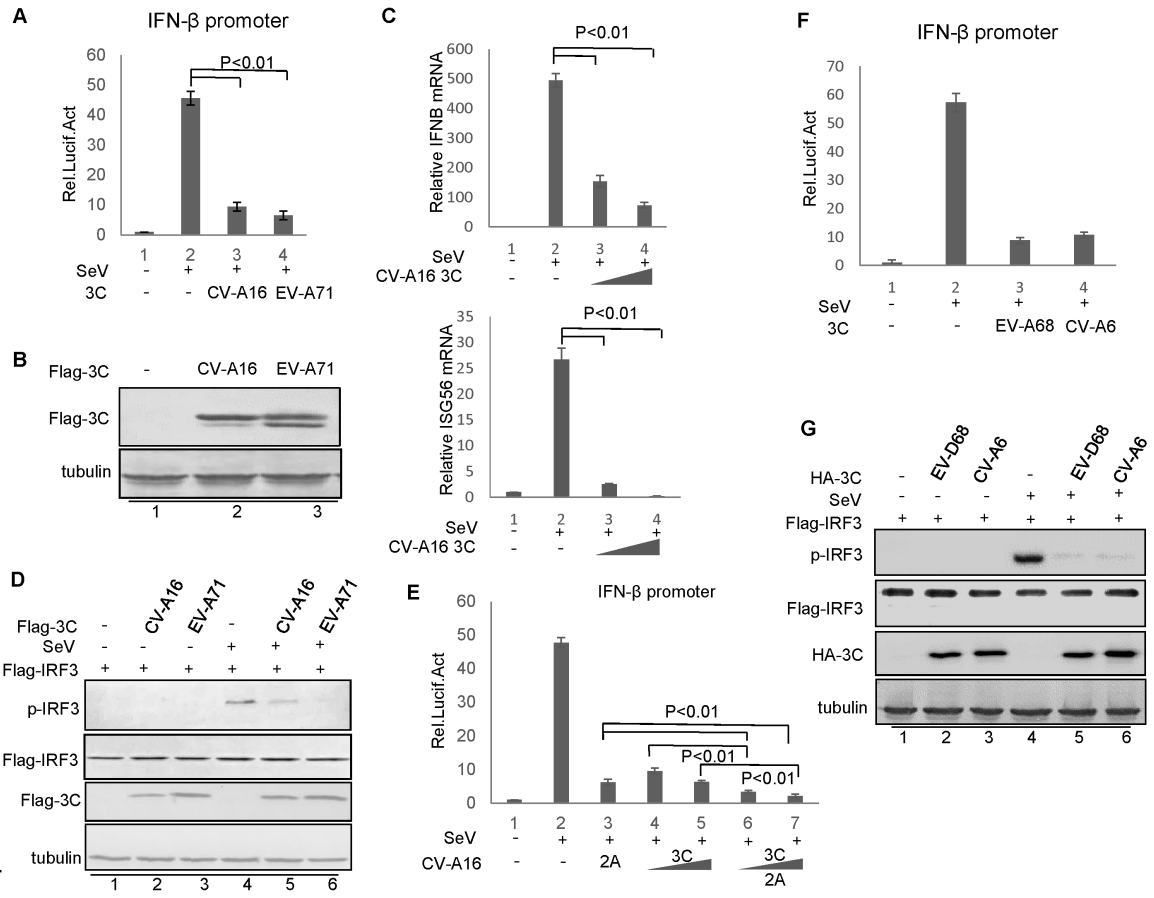

Fig. 4

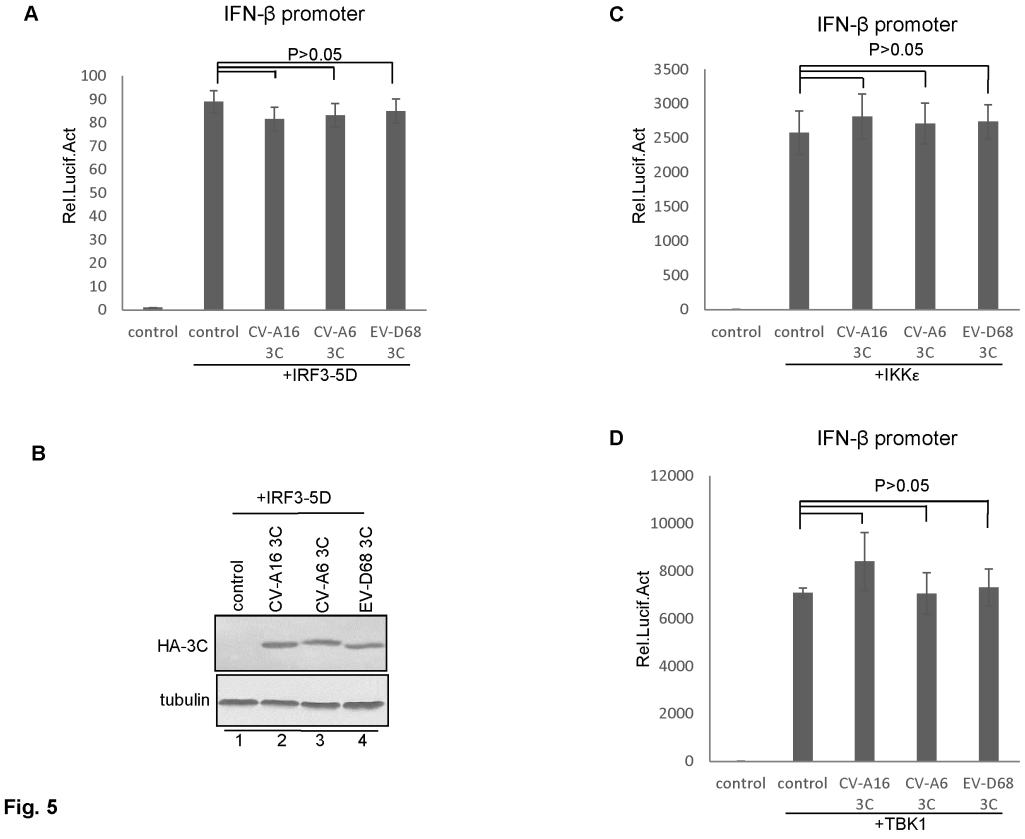

Fig. 5

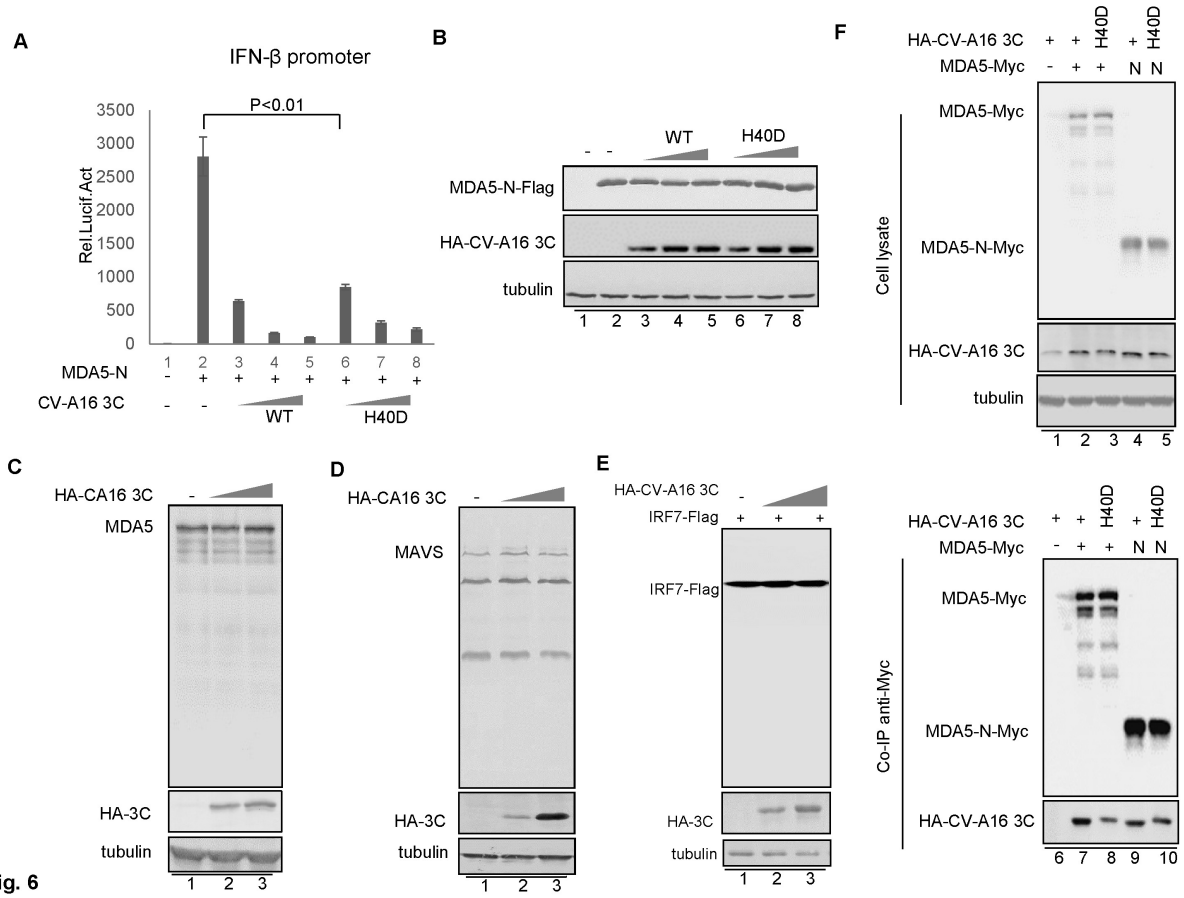

Fig. 6

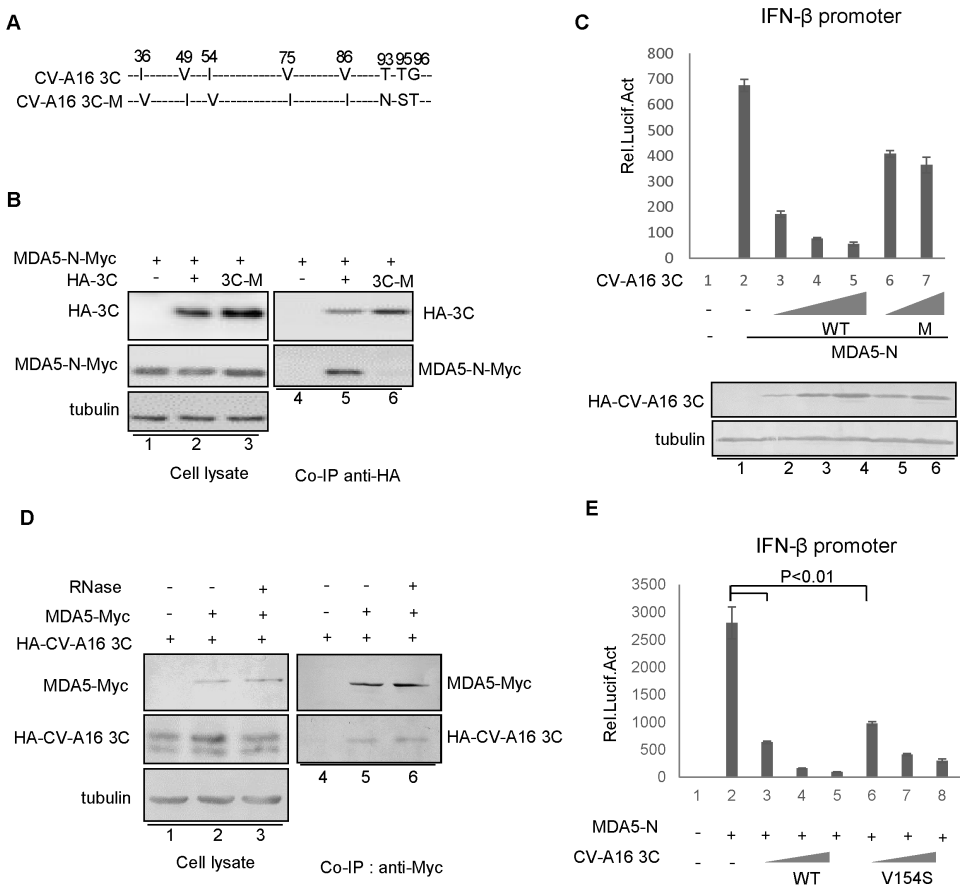

Fig. 7

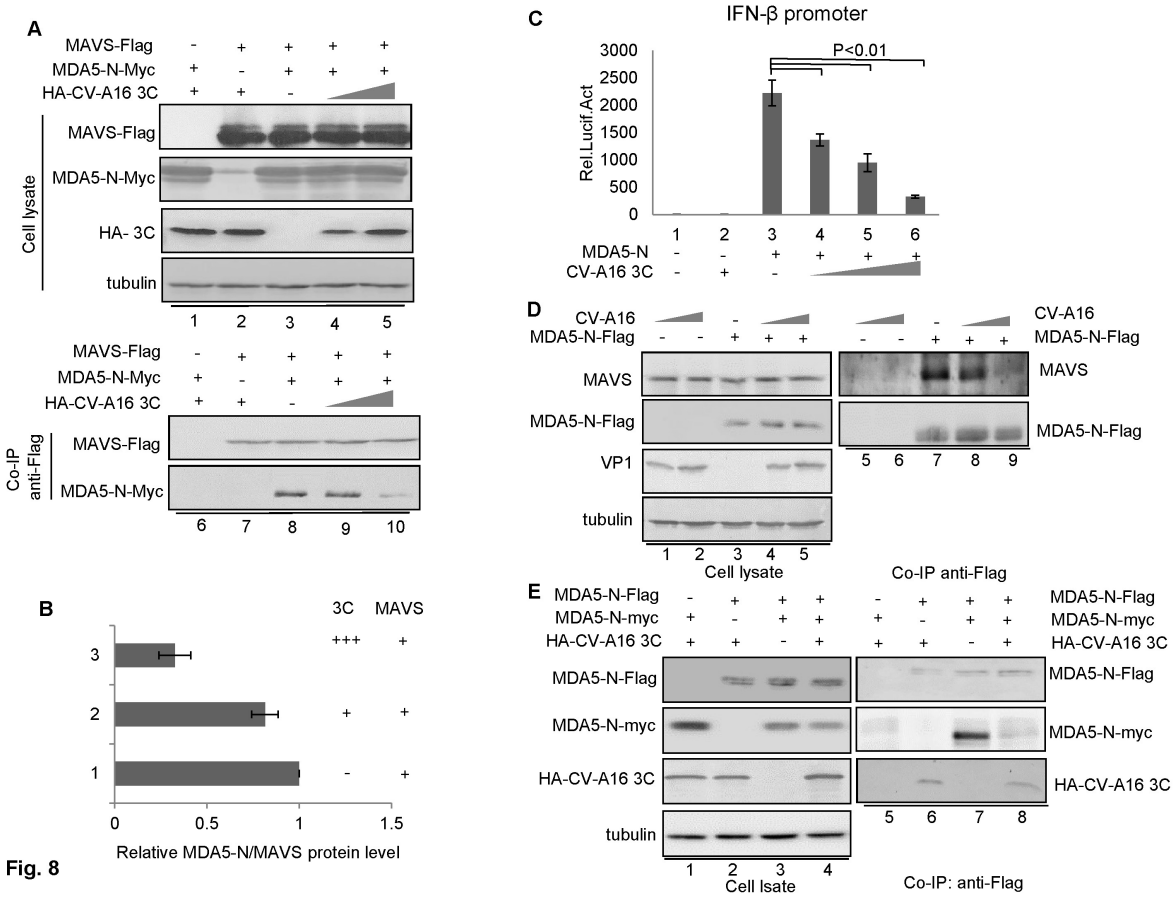

Fig. 8

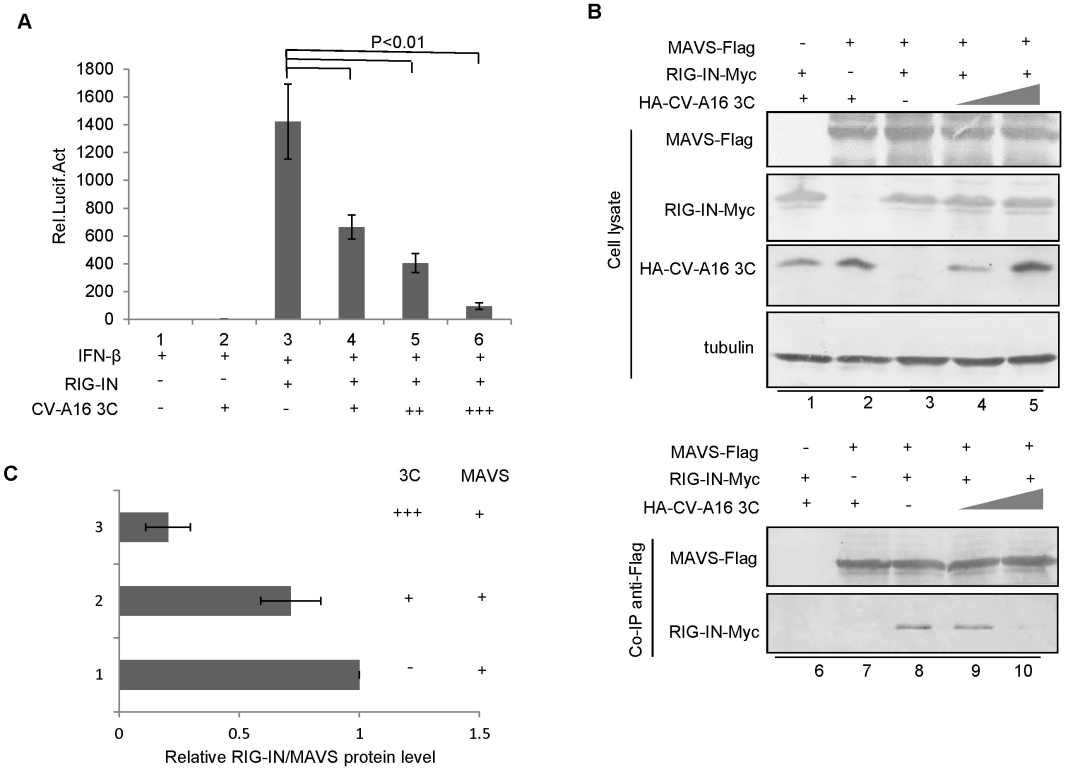

Fig. 9

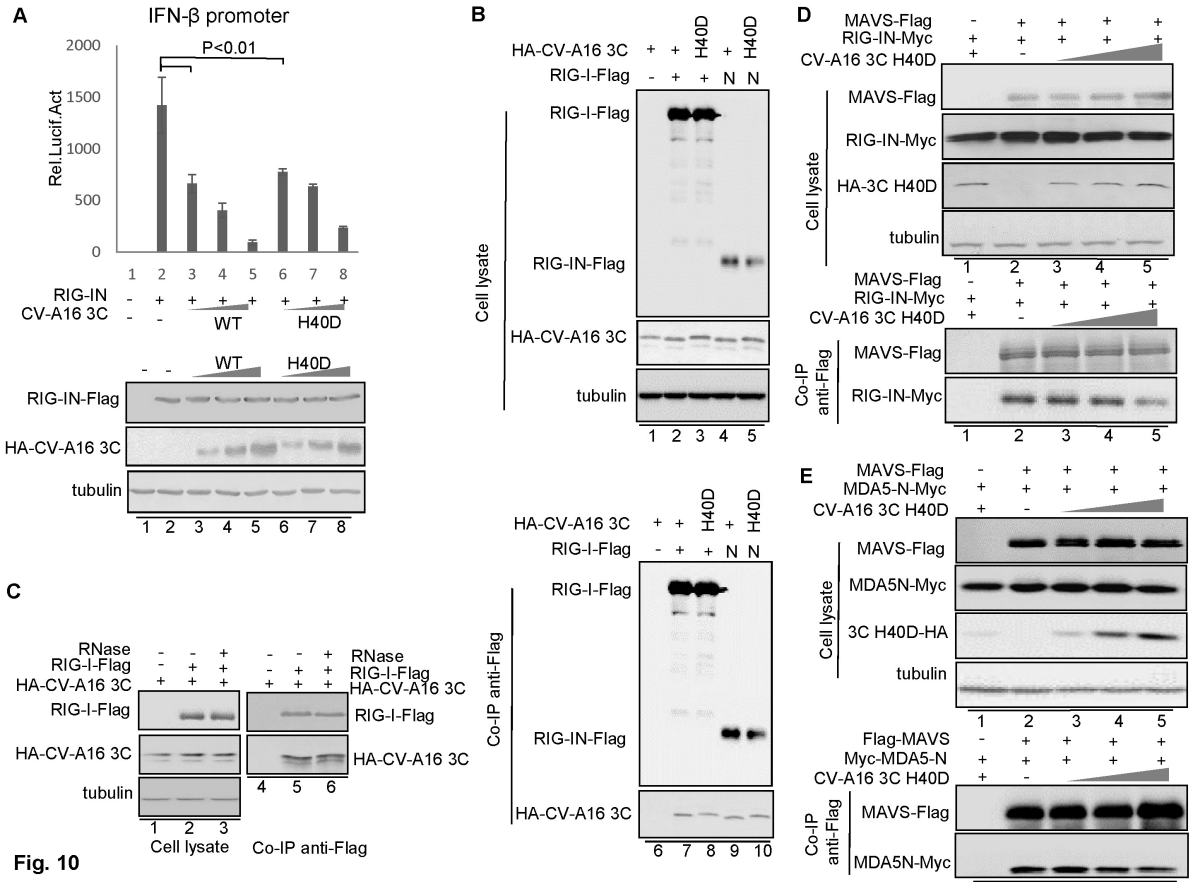

Fig. 10

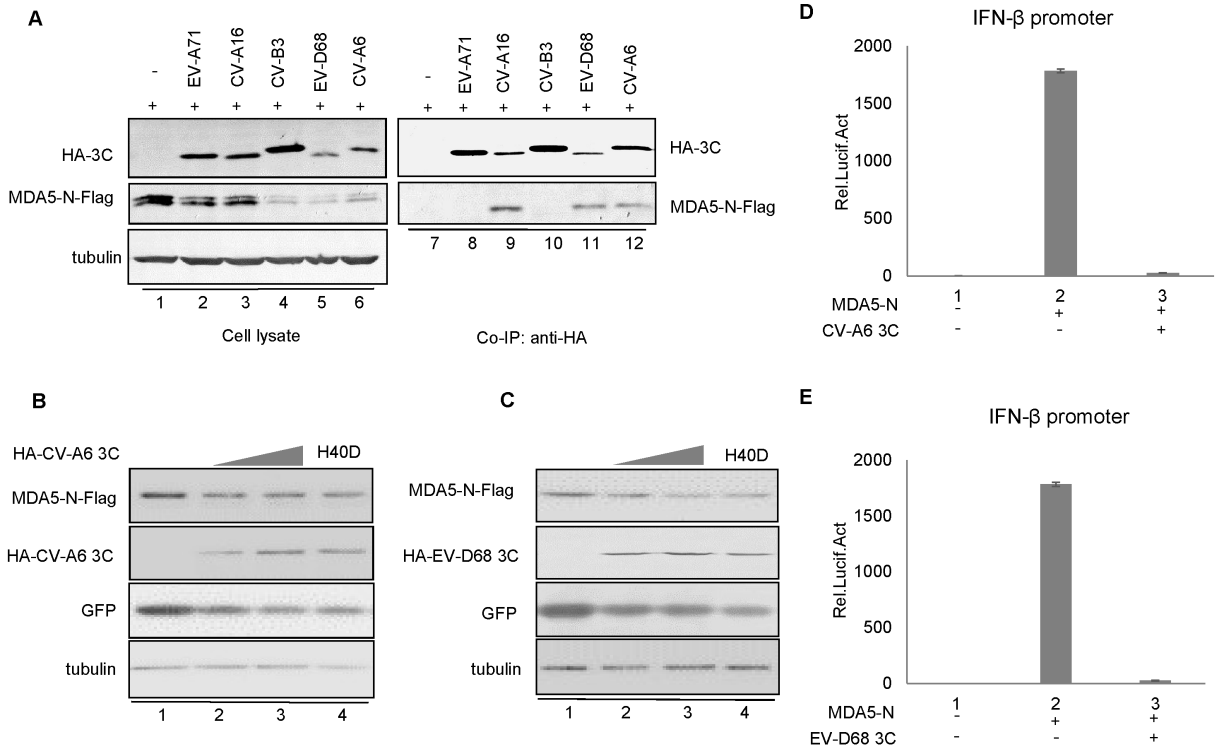

Fig. 11

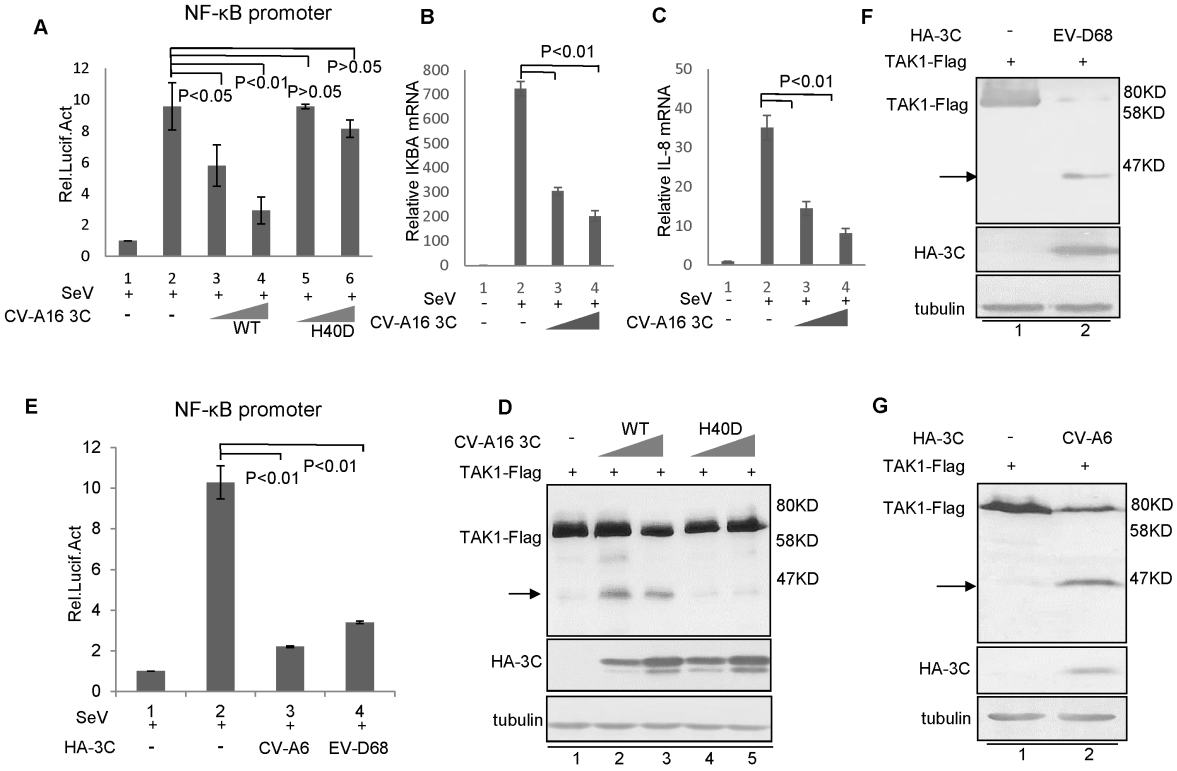

Fig. 12

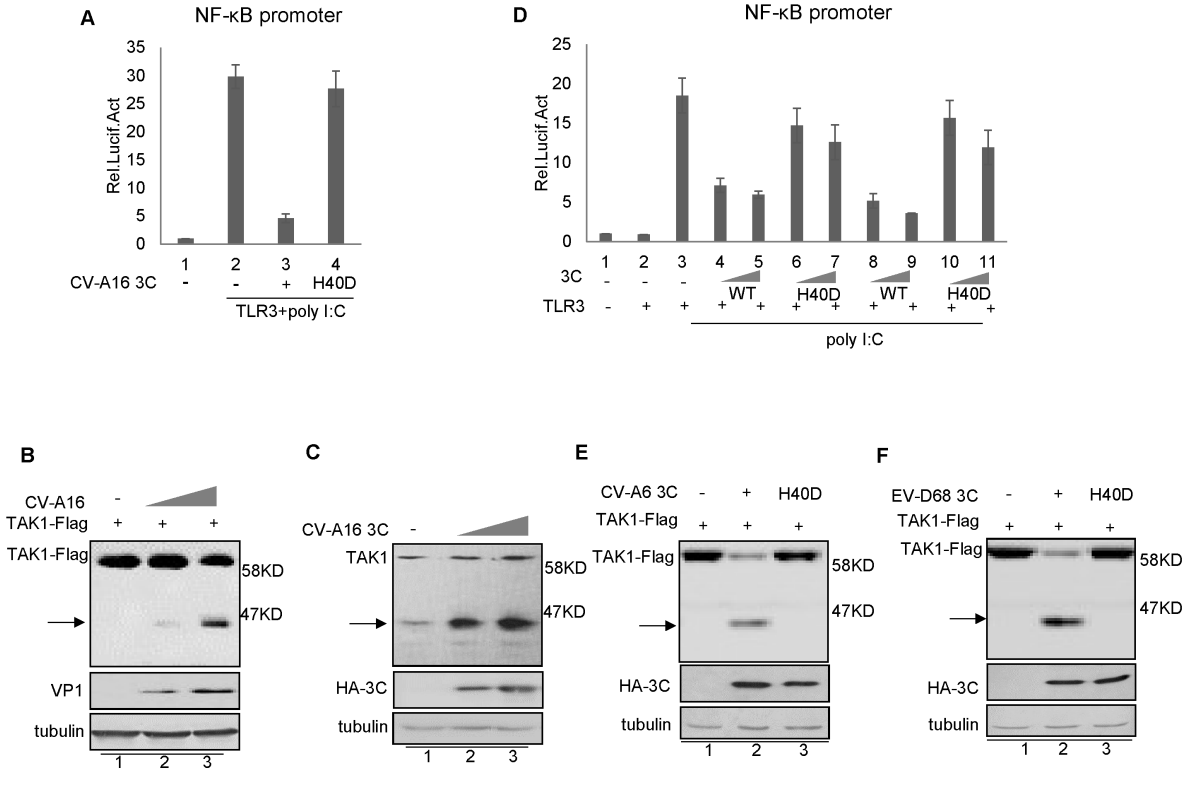

Fig. 13

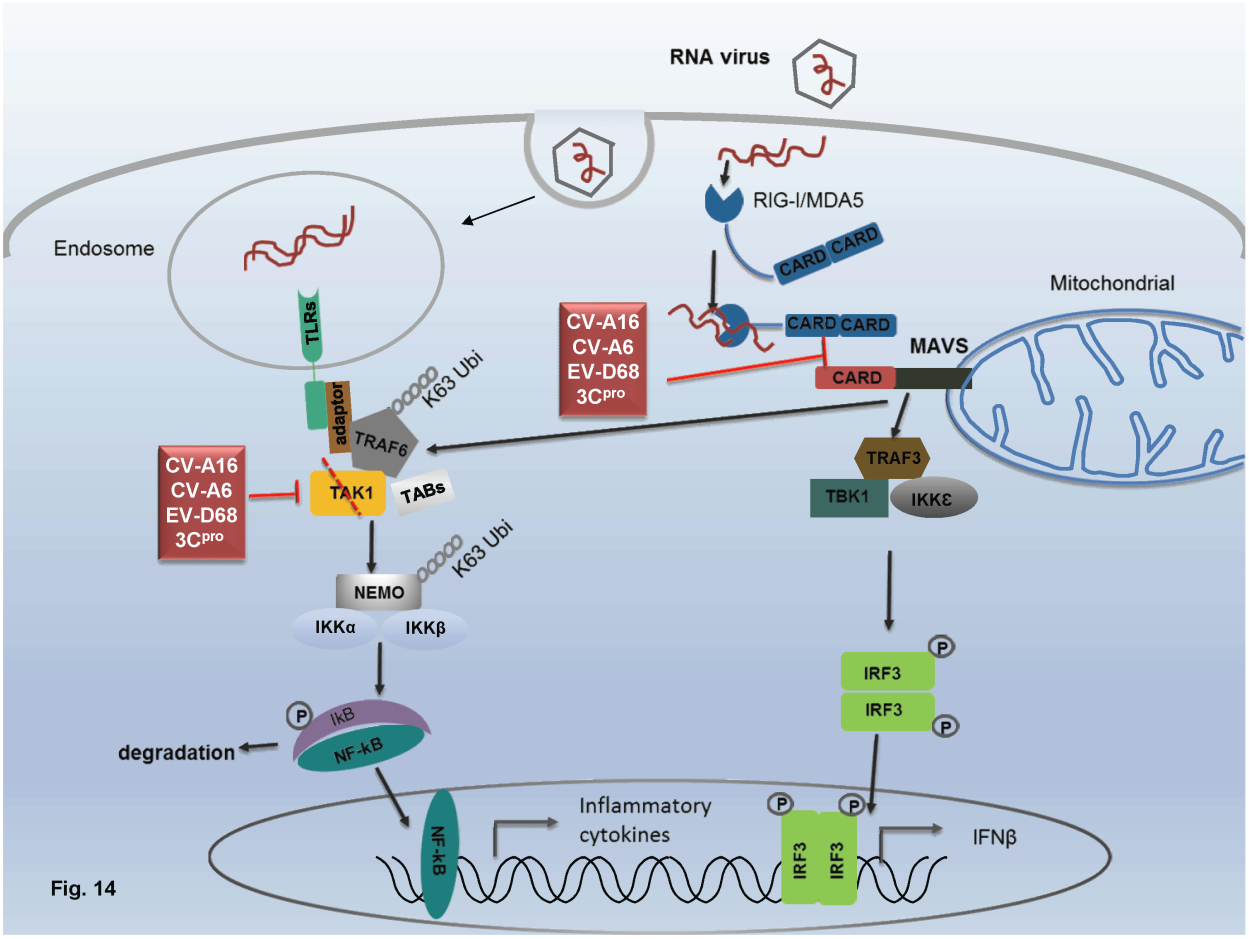

Fig. 14